A GALERKIN METHOD FOR LINEAR PDE SYSTEMS IN CIRCULAR GEOMETRIES WITH STRUCTURAL ACOUSTIC APPLICATIONS [1]

Ralph C. Smith
Department of Mathematics
Iowa State University
Ames, IA 50011

ABSTRACT

A Galerkin method for systems of PDE's in circular geometries is presented with motivating problems being drawn from structural, acoustic and structural acoustic applications. Depending upon the application under consideration, piecewise splines or Legendre polynomials are used when approximating the system dynamics with modifications included to incorporate the analytic solution decay near the coordinate singularity. This provides an efficient method which retains its accuracy throughout the circular domain without degradation at the singularity. Because the problems under consideration are linear or weakly nonlinear with constant or piecewise constant coefficients, transform methods for the problems are not investigated. While the specific method is developed for the 2-D wave equation on a circular domain and the equation of transverse motion for a thin circular plate, examples demonstrating the extension of the techniques to a fully coupled structural acoustic system are used to illustrate the flexibility of the method when approximating the dynamics of more complex systems.

[1]This research was supported in part by the National Aeronautics and Space Administration under NASA Contract Numbers NAS1-18605 and NAS1-19480 while the author was a visiting scientist at the Institute for Computer Applications in Science and Engineering (ICASE), NASA Langley Research Center, Hampton, VA 23681. Additional support was also provided in part under NASA grant NAG-1-1600.

1 Introduction

A common step in many structural, acoustic and fluid applications involves the solution of partial differential equations (PDE's) modeling the physics of a system having a circular geometry. Examples of applications in which this is important include the determination and control of circular plate and cylindrical shell dynamics, the modeling and attenuation of noise within a cylindrical cavity, the simulation of fluid flow and boundary layer growth in a pipe, as well as innumerable other applications involving circular domains. Due to the complexity of the problems, however, analytic solutions usually cannot be obtained and one must numerically approximate the dynamics under consideration.

From separation of variables and truncation of the resulting infinite series, approximations in the form of modal expansions involving Bessel components can occasionally be used to approximate PDE dynamics. However, modal expansions can be determined for only a limited number of applications and hence one must often employ more general techniques such as finite difference, finite element, spline, or spectral expansions in order to approximate the dynamics of the system under consideration.

In the category of spectral methods for circular geometries, Galerkin, collocation and tau methods have been studied with the choice of method depending upon the problem being considered. To date, much of this research has centered around the simulation of fluid flow and boundary layer growth and in these cases, emphasis has usually been placed on collocation due its success in handling complex boundary conditions, variable coefficients, and strong nonlinearities [16, 17]. Galerkin methods for flows on spheres are discussed in [15], but this is done primarily in the context of Fourier expansions involving the strong form of the modeling flow equations with only a brief discussion concerning Legendre bases being included. As noted in this latter reference, care must be exercised when applying any of the previously mentioned techniques (Galerkin, collocation or tau) to problems with coordinate singularities since the incorrect application of pole conditions can significantly degrade the accuracy of the method as well as introduce strong numerical instabilities. This reference also includes a general comparison between the results obtained with surface harmonics (eigenfunctions of the Laplacian), modified Robert functions and Fourier series using collocation and Galerkin methods in the presence of the coordinate singularity. The use of the modified Robert functions and techniques for improving their conditioning and employing fast transforms is further addressed in [10]. Finally, general overviews concerning the application of spectral methods to problems with coordinate singularities can be found in [11, 12]. We point out that the emphasis in these references centers primarily around the development of numerical methods for flows of various types and hence the techniques are often geared toward the approximation of strongly nonlinear operators which requires transform methods to facilitate efficient implementation. While these techniques will clearly work for linear problems involving circular domains, they often are not optimal nor the best choice for the applications under consideration.

In this paper, we present a Galerkin method for linear or weakly nonlinear problems having circular or cylindrical domains using piecewise spline and spectral bases. Two areas from which we will draw examples are structural dynamics and acoustics (a search of the literature reveals few numerical techniques for these types of problems on circular domains). Linearization in the first case is often justified when dealing with small amplitude vibrations while linearized

acoustic equations are often employed when considering acoustic fields having sound pressure levels less than 150 dB (which is the case in a large number of acoustic and structural acoustic applications). While weak nonlinearities of the type considered in [7] can also be efficiently implemented, the discussion here will concentrate on the linear case. Moreover, the coefficients in the problems of interest will be taken to be constant or piecewise constant in nature (this is certainly a reasonable assumption for many acoustic problems and a valid condition in a large class of structural applications). Hence we will not address the use of transform methods for evaluating variable coefficients and nonlinear components.

Throughout the discussion, the modeling equations will be approximated in the weak or variational form in accordance with energy formulations of the problems. In the structural application, this is done to reduce smoothness requirements on approximating elements and to accommodate structural and material discontinuities as well as unbounded (discontinuous) input operators. The consideration of the acoustic problem in weak form proves to be useful when considering coupled structural acoustic systems. Moreover, in weak form, some physical boundary conditions (e.g., the hard wall conditions which we consider here) are *natural* which implies that no basis alterations are necessary when implementing the method. We point out, however, that if the application warrants, approximation of the acoustic dynamics using the strong form of the system equations can just as efficiently be accomplished using the techniques of the paper. Moreover, these techniques can be easily modified to accommodate a tau method if dealing with more complex *essential* boundary conditions (boundary conditions which must be explicitly satisfied in a variational formulation of the problem).

In the second section of this paper, a 2-D acoustic problem on a circular domain is considered with a Fourier-Legendre basis being used in the ensuing approximations. In addition to its accuracy, the use of this basis proves to be advantageous in control applications since it facilitates the maintenance of uniform stability margins under approximation [4]. Moreover, the the use of the spectral basis facilitates approximation in a quotient space which is often the natural state space in acoustic problems.

The techniques are then applied to a structural application in Section 3 with the problem of approximating circular plate dynamics being used to motivate the analysis. In this case, cubic splines modified to satisfy boundary conditions are used in conjunction with a Fourier basis to obtain a suitable finite-dimensional approximation to the problem. The use of splines rather than a spectral basis is motivated by smoothness requirements as well as the ease with which they can be adapted to satisfy *essential* boundary conditions, and can easily be changed if warranted by the form of the modeling equations and boundary conditions. We emphasize that when developing a general technique that could be applied in both cases, care was taken to treat the coordinate singularity in a manner that prevented degradation of accuracy using either basis (spectral or piecewise splines) as well as avoided the introduction of spurious numerical instabilities.

The techniques from Sections 2 and 3 are then combined in Section 4 where the problem of approximating the dynamics of a fully coupled structural acoustic system is considered. This demonstrates the flexibility of the method when studying a more complex coupled physical system and illustrates the manner through which the basic techniques can be extended to more general problems. The convergence properties of the method and its use in determining physical properties of the system are illustrated through a set of examples. Finally, advantages of the method in control applications are discussed in the concluding remarks.

2 The Wave Equation

In this section we consider the 2-D wave equation on a circular domain Ω of radius a with the boundary denoted by Γ. For Neumann boundary constraints and initial conditions ϕ_0 and ϕ_1, the equations of motion are

$$\begin{aligned} &\phi_{tt} = c^2\Delta\phi + g(t,r,\theta) \quad , \quad (r,\theta) \in \Omega \ , t > 0 \ , \\ &\nabla\phi \cdot \hat{r} = 0 \quad , \quad (r,\theta) \in \Gamma \ , t > 0 \ , \\ &\phi(0,r,\theta) = \phi_0(r,\theta) \quad , \quad (r,\theta) \in \Omega \ , \\ &\phi_t(0,r,\theta) = \phi_1(r,\theta) \quad , \quad (r,\theta) \in \Omega \end{aligned} \tag{2.1}$$

where ϕ, in acoustics applications [14], denotes the velocity potential and c is the speed of sound. We note that the Neumann boundary conditions are chosen so as to be consistent with the hard wall conditions in the physical application described in Section 4 and can be altered to fit the individual problems under investigation.

To gain insight into the behavior of the solution and to motivate the form of the approximation, we first solve the equations analytically through a standard separation of variables. For the homogeneous problem ($g = 0$), we take $\phi(t,r,\theta) = T(t)\Phi(r,\theta)$ to arrive at the two dimensional Helmholz equation

$$\begin{aligned} &\Delta\Phi + \gamma^2\Phi = 0 \quad , \ (r,\theta) \in \Omega \ , \\ &\nabla\Phi \cdot \hat{r} = 0 \quad , \ (r,\theta) \in \Gamma \end{aligned} \tag{2.2}$$

and the relation $T'' + \omega^2 T = 0 \ , \ t > 0$. The separation constant here is $-\gamma^2 = -(\frac{\omega}{c})^2$ where ω is the circular frequency with units of radians/sec. To find Φ, we separate variables once more. Letting $\Phi(r,\theta) = R(r)\Theta(\theta)$, the expansion of Helmholz's equation yields the expression

$$\frac{1}{rR}\frac{d}{dr}\left(r\frac{dR}{dr}\right) + \frac{1}{r^2\Theta}\frac{d^2\Theta}{d\theta^2} + \gamma^2 = 0$$

which implies that R and Θ must satisfy the differential equations

$$\begin{aligned} &R'' + \frac{1}{r}R' + \left(\gamma^2 - \frac{m^2}{r^2}\right)R = 0 \\ &R'(a) = 0 \ , \end{aligned} \tag{2.3}$$

and

$$\begin{aligned} &\Theta'' + m^2\Theta = 0 \\ &\Theta(0) = \Theta(2\pi) \ . \end{aligned} \tag{2.4}$$

The general solution to (2.4) is periodic and is given by $\Theta(\theta) = A_1 e^{im\theta}, m = 0, \pm 1, \pm 2, \cdots$. Moreover, the general solution of the Bessel equation (2.3) is $R(r) = A_2 J_m(\gamma r) + A_3 Y_m(\gamma r)$ where J_m and Y_m are the m^{th} Bessel functions of the first and second kind, respectively. As noted in [1], these functions display the asymptotic behavior

$$J_m(z) \sim \frac{z^m}{2^m m!} \quad , \quad Y_m(z) \sim -\frac{2^m(m-1)!}{\pi z^m} \tag{2.5}$$

for fixed m and $z \to 0$. Because Y_m grows unboundedly at the origin, we take $A_3 = 0$ in order to guarantee that the solution remains bounded at $r = 0$. The decay properties of J_m will be incorporated when developing an approximation method for the problem.

The eigenvalues γ_{mn} of (2.2) are then determined by applying the boundary condition and solving for the zeros of the nonlinear equation

$$\frac{dJ_m(\gamma a)}{dr} = 0 \ . \tag{2.6}$$

The corresponding eigenvectors or modes are $\Psi_{mn}(r,\theta) = J_m(\gamma_{mn} r)e^{im\theta}$ for $m = 0, \pm 1, \pm 2, \cdots$, $n = 1, 2, 3, \cdots$ which implies that standing waves have the form

$$\phi_{mn}(t,r,\theta) = \left[a_n \sin(\gamma_{mn} ct) + b_n \cos(\gamma_{mn} ct)\right] J_m(\gamma_{mn} r)e^{im\theta} \ .$$

A variation of parameters approach can then be used to extend this to the nonhomogeneous case. With suitable smoothness assumptions on the initial conditions and forcing term, it can be shown that the solution to (2.1) has the form

$$\phi(t,r,\theta) = \sum_{m=-\infty}^{\infty} \sum_{n=1}^{\infty} \phi_{mn}(t) J_m(\gamma_{mn} r)e^{im\theta} \tag{2.7}$$

where the coefficients $\phi_{mn}(t)$ depend on ϕ_0, ϕ_1 and the time-dependent Fourier coefficients of g (we refer the reader to any standard PDE text for details concerning the justification of the formal calculations outlined here).

Having outlined the arguments leading to the analytic form of the solution, we now want to use those results to motivate an appropriate Galerkin technique for approximating the solution. To facilitate the use of this scheme in coupled structural acoustic systems (see, for example, the system discussed in Section 4), the weak form of the system equations will be considered. Moreover, to illustrate the use of the method when approximating the acoustic potential (which is determined to within only a constant [14]), a basis suitable for a quotient space will be chosen.

To pose the system (2.1) in weak form, we take the state to be ϕ in the space $H = \bar{L}^2(\Omega)$ where $\bar{L}^2(\Omega)$ is the quotient space of L^2 over the constant functions. The space of test functions is taken to be the quotient space $V = \bar{H}^1(\Omega)$. The inner products for the two spaces are taken to be

$$\langle \phi, \xi \rangle_H = \int_\Omega \frac{1}{c^2} \phi \bar{\xi} d\omega \quad , \quad \langle \phi, \xi \rangle_V = \int_\Omega \nabla \phi \cdot \overline{\nabla \xi} d\omega$$

(the overbars here denote complex conjugation as compared with those used above to delineate the quotient spaces). Energy considerations or integration by parts then yields the variational form

$$\int_\Omega \phi_{tt} \overline{\xi} d\omega + \int_\Omega \nabla \phi \cdot \overline{\nabla \xi} d\omega = \int g \overline{\xi} d\omega \tag{2.8}$$

for all ξ in V.

To discretize, we begin with a Fourier expansion in θ which yields the approximate solution

$$\phi^{\mathcal{M}}(t,r,\theta) = \sum_{m=-M}^{M} \tilde{\phi}_m(t,r)e^{im\theta} \ . \tag{2.9}$$

We point out that the use of the complex Fourier expansion simplifies the following discussion both in describing the form of the approximate solution and the construction of the system matrices. However, when combining these wave results with those of the circular plate to yield an approximation scheme for the coupled system (see Section 4), it is easier to use a real Fourier expansion when performing the actual computations (this is due to the presence of the piezoceramic patches on the plate). The interchange between the two expansions is straightforward, and hence details concerning the implementation of the real Fourier scheme are left to the reader.

Several possibilities exist for spline, Legendre or Chebyshev expansions of $\tilde{\phi}_m(t,r)$ both in a collocation and Galerkin setting. These include direct expansions which maintain the parity of the solution, refinements to incorporate the decay of the solution at the origin, and mapped expansions which use all the polynomials and yield better center resolution. These expansions must satisfy the condition

$$\frac{\partial \phi^{\mathcal{M}}}{\partial \theta} = 0$$

at the origin which guarantees the uniqueness of the solution. This yields the requirement

$$\tilde{\phi}_m(t,r) = 0 \qquad \text{at } r = 0 \ , \ m \neq 0 \ . \tag{2.10}$$

To guarantee differentiability at the origin, it is appropriate to require that the remaining component satisfies

$$\frac{\partial \tilde{\phi}_0}{\partial r} = 0 \qquad \text{at } r = 0 \ . \tag{2.11}$$

As detailed in [6], one expansion of $\tilde{\phi}_m(t,r)$ which satisfies these properties is

$$\tilde{\phi}_m(t,r) = \sum_{n=0}^{N^m} \phi_{mn}(t) r^{|\hat{m}|} P_n^m(r)$$

where

$$\hat{m} = \begin{cases} m & , \quad |m| = 0, \cdots, 5 \\ 5 & , \quad |m| = 6, \cdots, M \end{cases} \tag{2.12}$$

and

$$P_n^m(r) = \begin{cases} P_1(r) - 1/3 & , \quad m = 0, n = 1 \\ P_n(r) & , \quad \text{otherwise} \ . \end{cases}$$

Here $P_n(r)$ is the n^{th} Legendre polynomial which has been mapped to the interval $(0,a)$. The term $P_1(r) - 1/3$ when $m = 0, n = 1$ results from the orthogonality properties of the Legendre polynomials and arises when enforcing the condition $\int_\Omega \phi^{\mathcal{M}}(t,r,\theta,z) d\omega = 0$ so as to guarantee that the functions are suitable as a basis for the quotient space. The inclusion of the weight $r^{|\hat{m}|}$ incorporates the decay of the analytic solution near the origin (see (2.5)) while ensuring its uniqueness at that point. Finally, we note that if N Legendre functions are used, the limit N^m is given by $N^m = N + 1$ when $|m| \neq 0$ and $N^m = N$ when $m = 0$, which implies that $\mathcal{M} = (2M+1)(N^m+1) - 1$ basis functions are used in the wave expansion.

Summarizing, the approximate solution to (2.8) can be expressed as

$$\phi^{\mathcal{M}}(t,r,\theta) = \sum_{m=-M}^{M} \sum_{n=1}^{N^m} \phi_{mn}(t) r^{|\hat{m}|} P_n^m(r) e^{im\theta} = \sum_{k=1}^{\mathcal{M}} \phi_k(t) B_k^{\mathcal{M}}(r,\theta) \tag{2.13}$$

where $B_k^{\mathcal{M}}(r,\theta) = r^{|\hat{m}|}P_n^m(r)e^{im\theta}$. In comparing the form of this approximate solution with the analytic wave solution defined in (2.7), it can be seen that we have essentially replaced the Bessel components by weighted Legendre functions. This provides an approximate solution which is more flexible and is quicker to converge in a variety of applications than that obtained with a purely eigenfunction expansion (indeed, for more complex systems involving wave components, the eigenfunctions are unavailable and would have to be approximated before they could be used as a basis).

To provide an approximating finite-dimensional space for the problem, we define the subspace $H^{\mathcal{M}} = span\{B_k^{\mathcal{M}}\}$ and take the product space for the first-order problem to be $\mathcal{H}^{\mathcal{M}} = H^{\mathcal{M}} \times H^{\mathcal{M}}$. The restriction of the infinite-dimensional system (2.8) to the space $\mathcal{H}^{\mathcal{M}} \times \mathcal{H}^{\mathcal{M}}$ then yields

$$\int_\Omega \frac{1}{c^2}\phi_{tt}^{\mathcal{M}}\bar{\xi}d\omega + \int_\Omega \nabla\phi^{\mathcal{M}} \cdot \overline{\nabla\xi}d\omega = \int_\Omega \frac{1}{c^2}g\bar{\xi}d\omega$$

for ξ in $H^{\mathcal{M}}$. The corresponding matrix system is

$$\begin{aligned}
&\begin{bmatrix} K_{r\theta}^{\mathcal{M}} & 0 \\ 0 & M_{r\theta}^{\mathcal{M}} \end{bmatrix} \begin{bmatrix} \dot{\vartheta}^{\mathcal{M}}(t) \\ \ddot{\vartheta}^{\mathcal{M}}(t) \end{bmatrix} = \begin{bmatrix} 0 & K_{r\theta}^{\mathcal{M}} \\ -K_{r\theta}^{\mathcal{M}} & 0 \end{bmatrix} \begin{bmatrix} \vartheta^{\mathcal{M}}(t) \\ \dot{\vartheta}^{\mathcal{M}}(t) \end{bmatrix} + \begin{bmatrix} 0 \\ \tilde{G}_2^{\mathcal{M}}(t) \end{bmatrix} \\
&\begin{bmatrix} K_{r\theta}^{\mathcal{M}} & 0 \\ 0 & M_{r\theta}^{\mathcal{M}} \end{bmatrix} \begin{bmatrix} \vartheta^{\mathcal{M}}(0) \\ \dot{\vartheta}^{\mathcal{M}}(0) \end{bmatrix} = \begin{bmatrix} g_1^{\mathcal{M}} \\ g_2^{\mathcal{M}} \end{bmatrix}
\end{aligned} \tag{2.14}$$

where $\vartheta^{\mathcal{M}}(t) = [\phi_1(t), \phi_2(t), \cdots, \phi_{\mathcal{M}}(t)]^T$ denotes the $\mathcal{M} \times 1$ vector containing the approximate state coefficients. The component matrices and vectors are given by

$$\begin{aligned}
\left[K_{r\theta}^{\mathcal{M}}\right]_{\ell,k} &= \int_\Omega \nabla B_k^{\mathcal{M}} \cdot \overline{\nabla B_\ell^{\mathcal{M}}}d\omega \ , \\
\left[M_{r\theta}^{\mathcal{M}}\right]_{\ell,k} &= \int_\Omega \frac{1}{c^2}B_k^{\mathcal{M}}\overline{B_\ell^{\mathcal{M}}}d\omega \ , \\
\left[\tilde{G}_2^{\mathcal{M}}(t)\right]_\ell &= \int_\Omega \frac{1}{c^2}g\overline{B_\ell^{\mathcal{M}}}d\omega \ , \\
\left[g_1^{\mathcal{M}}\right]_\ell &= \int_\Omega \nabla\phi_0 \cdot \overline{\nabla B_\ell^{\mathcal{M}}}d\omega = \left\langle \phi_0, B_\ell^{\mathcal{M}} \right\rangle_V \ , \\
\left[g_2^{\mathcal{M}}\right]_\ell &= \int_\Omega \frac{1}{c^2}\phi_1\overline{B_\ell^{\mathcal{M}}}d\omega = \left\langle \phi_1, B_\ell^{\mathcal{M}} \right\rangle_H
\end{aligned} \tag{2.15}$$

where the index ranges are $k, \ell = 1, \cdots, \mathcal{M}$. We note that the presence of the matrix $K_{r\theta}^{\mathcal{M}}$ in the $\dot{\vartheta}^{\mathcal{M}}$ component of (2.14) and mass matrix is due to the form of the V-inner product.

We point out that the Fourier-Galerkin technique leading to the matrix system (2.14) is quite general in nature and can be used to approximate wave solutions in cases where the analytic solutions described at the beginning of this section are unavailable or impractical to use. The general techniques described here are also easily adapted to different boundary conditions and more complex systems involving acoustic components. Test cases illustrating the basic method are given in the following examples and the extension of these techniques to a more complex coupled structural acoustic system is presented in Section 4.

2.1 Example 1

As a first test of this approximation method, we considered the forced wave equation

$$\begin{aligned} \phi_{tt} &= c^2\Delta\phi + g(t,r,\theta) \quad , \quad (r,\theta) \in \Omega \ , t > 0 \ , \\ \nabla\phi \cdot \hat{r} &= 0 \quad , \quad (r,\theta) \in \Gamma \ , t > 0 \ , \\ \phi(0,r,\theta) &= \phi_t(0,r,\theta) = 0 \quad , \quad (r,\theta) \in \Omega \end{aligned}$$

on the circular domain Ω of radius $a = 1$. The true solution $\phi(t,r,\theta) = t^2[\cos(2\pi r)-1]^2[\sin(3\theta)+\cos(\theta)]$ was used to generate the forcing function g, and the problem was then discretized to yield the matrix system (2.14). The absolute and relative errors obtained by integrating this system to time $T = 1$ and comparing with the known true solution on a uniform mesh are recorded in Table 1. The true solution at that time is depicted in Figure 1 while line plots comparing the approximate and true solutions along the central line $\ell = \{(x,y) : -1 \le x \le 1, y = 0\}$ are given in Figure 2.

The solution for this problem was chosen in a manner that allowed us to fix the Fourier limit and examine the convergence as the Galerkin limit was increased. The rapid convergence exhibited by the results in Table 1 is consistent with that expected from the radial Legendre basis. A slight decrease in the convergence rate is noted when $N = 15$, and we believe that this is due to error in time discretization rather than spatial approximation (a standard fourth/fifth order Runge-Kutta routine was used to integrate the system). In this and other examples that we have examined, it can be noted that as long as the solution being approximated is sufficiently smooth at the origin, the approximation method performs well and accurate results can be obtained with a relatively small number of basis functions. For example, the plots in Figure 2 demonstrate that while small oscillations near the origin are present in the approximate solutions obtained with $N = 3$ and $N = 6$, they are gone with larger discretization limits and if fact, the approximate solution obtained with $N = 9$ is graphically indistinguishable from the true solution. For less smooth functions (e.g., functions that are only continuous and differentiable at the origin), some loss of accuracy does occur, although, in applications this has not been a factor since these types of discontinuities generally do not occur in the physical systems whose dynamics we are simulating.

M	N	$2\mathcal{M}$	$\|\phi_{true} - \phi_{app}\|$	$\frac{\|\phi_{true}-\phi_{app}\|}{\|\phi_{true}\|}$
3	3	54	$1.0067 - 0$	$.1357 - 0$
3	6	96	$.1453 - 0$	$.1959 - 1$
3	9	138	$.1269 - 2$	$.1710 - 3$
3	12	180	$.8567 - 4$	$.1155 - 4$
3	15	222	$.1912 - 4$	$.2578 - 5$

Table 1. Absolute and relative errors when approximating the wave solution $\phi(t,r,\theta) = t^2[\cos(2\pi r) - 1]^2[\sin(3\theta) + \cos(\theta)]$.

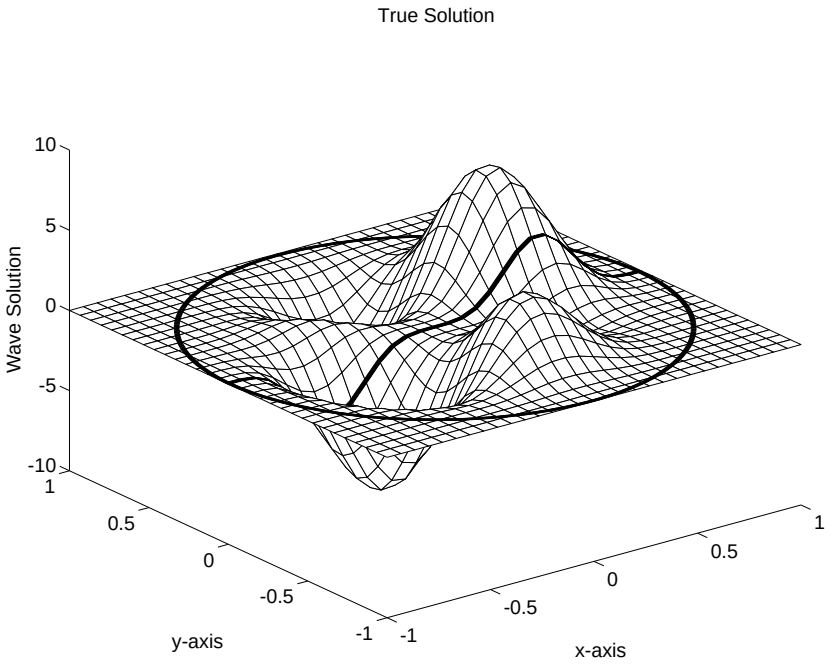

Figure 1. True solution $\phi(t, r, \theta) = t^2[\cos(2\pi r) - 1]^2[\sin(3\theta) + \cos(\theta)]$ at time $T = 1$.

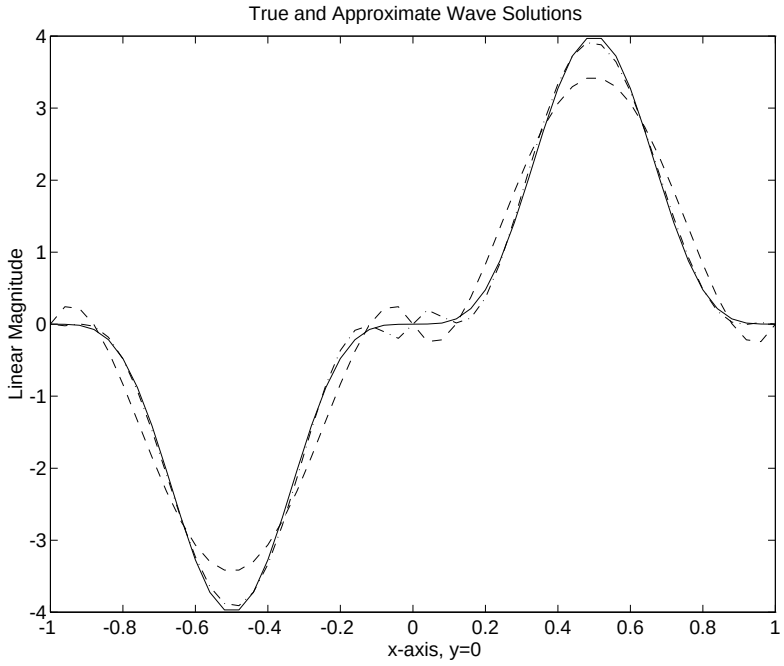

Figure 2. True and approximate solutions, – – – $(N = 3)$, – · – $(N = 6)$, ——— (True).

2.2 Example 2

A second means of testing the accuracy of the mass and stiffness matrices in the system (2.14) and hence checking the accuracy and convergence properties of the approximation method is by discretizing the eigenvalue problem

$$\begin{aligned} \Delta\Phi + \gamma^2\Phi = 0 \quad &, \ (r,\theta) \in \Omega \ , \\ \nabla\Phi \cdot \hat{r} = 0 \quad &, \ (r,\theta) \in \Gamma \end{aligned}$$

(see (2.2)) which arises when separating variables in the homogeneous wave equation. As discussed previously, the eigenvalues γ_{mn} are determined by solving for the zeros of the nonlinear system $\frac{dJ_m(\gamma a)}{dr} = 0$ where J_m is the m^{th} Bessel function of the first kind. Several values obtained with $a = 1$ are summarized in Table 2 (see page 343 of [9] for details).

To compare these results with those obtained via the Fourier-Galerkin expansion, it is noted that under approximation in weak form, the eigenvalue problem (2.2) yields the generalized matrix eigenvalue problem

$$K_{r\theta}^{\mathcal{M}} \vartheta^{\mathcal{M}} = \gamma^2 M_{r\theta}^{\mathcal{M}} \vartheta^{\mathcal{M}} \tag{2.16}$$

with $c^2 = a = 1$ in the mass and stiffness matrices $M_{r\theta}^{\mathcal{M}}$ and $K_{r\theta}^{\mathcal{M}}$, respectively (see (2.15) for the definition of these matrices). The approximate eigenvalues obtained by solving (2.16) are summarized in Tables 3 and 4 for the limit choices $M = 6, N = 6$ and $M = 6, N = 12$, respectively. With the first choice of limits, it becomes difficult to distinguish the higher order eigenvalues and these are omitted from the table. We first note that with $M = 6, N = 12$, very accurate approximations are obtained with the largest relative error (4.4×10^{-4}) occurring when $m = n = 6$. Moreover, we see that while the definition of the modified Fourier component $\hat{m}$ (see (2.12)), which incorporates the analytic decay of the Laplacian near the origin, changes at $m = 5$, this has not reduced the accuracy of the method. Hence this example further illustrates the efficiency and accuracy of this approximation method for the wave equation on a circular domain.

n	$m=0$	$m=1$	$m=2$	$m=3$	$m=4$	$m=5$	$m=6$
0		1.8412	3.0542	4.2012	5.3176	6.4156	7.5013
1	3.8317	5.3314	6.7061	8.0152	9.2824	10.5199	11.7349
2	7.0156	8.5363	9.9695	11.3459	12.6819	13.9872	15.2682
3	10.1735	11.7060	13.1704	14.5858	15.9641	17.3128	18.6374
4	13.3237	14.8636	16.3475	17.7887	19.1960	20.5755	21.9317
5	16.4706	18.0155	19.5129	20.9725	22.4010	23.8036	25.1839
6	19.6159	21.1644	22.6716	24.1449	25.5898	27.0103	28.4098

Table 2. Values of γ_{mn} obtained from the Bessel condition $\frac{dJ_m(\gamma)}{dr} = 0$.

n	$m=0$	$m=1$	$m=2$	$m=3$	$m=4$	$m=5$	$m=6$
0		1.8412	3.0542	4.2012	5.3176	6.4156	7.5013
1	3.8317	5.3314	6.7061	8.0152	9.2824	10.5199	11.7349
2	7.0159	8.5378	9.9714	11.3472	12.6823	13.9874	15.2709
3	10.2668	11.7350	13.1858	14.6280	16.0386	17.4007	18.7540
4	13.7669	15.2709	17.2673	18.3866			

Table 3. Values of γ_{mn} obtained with $M = 6$, $N = 6$ Fourier-Galerkin basis functions.

n	$m=0$	$m=1$	$m=2$	$m=3$	$m=4$	$m=5$	$m=6$
0		1.8412	3.0542	4.2012	5.3176	6.4156	7.5013
1	3.8317	5.3314	6.7061	8.0152	9.2824	10.5199	11.7349
2	7.0156	8.5363	9.9695	11.3459	12.6819	13.9872	15.2682
3	10.1735	11.7060	13.1704	14.5858	15.9641	17.3128	18.6374
4	13.3237	14.8636	16.3475	17.7888	19.1960	20.5755	21.9317
5	16.4717	18.0159	19.5131	20.9730	22.4018	23.8043	25.1860
6	19.6250	21.1860	22.6929	24.1559	25.5937	27.0152	28.4223

Table 4. Values of γ_{mn} obtained with $M = 6$, $N = 12$ Fourier-Galerkin basis functions.

3 The Plate Equation

A second area in which one must commonly approximate the dynamics of PDE-based models posed on circular domains occurs when numerically simulating structural dynamics. While the assumption of small amplitude vibrations often leads to linear models, these models are often sufficiently complex so as to warrant special numerical techniques to capture the physics of the system. As a motivating example, we consider a thin circular plate having piezoceramic patches bonded in pairs to its surface (see Figure 3). When a voltage is applied to the patches, stresses are generated which can be used to invoke in-plane forces and/or bending moments in the underlying structure [8]. In this manner, the patches can be used to control plate vibrations [2] or acoustic sound pressure levels when the plate is an active component in a structural acoustic system [3, 4, 5]. For the analysis which follows, we assume that the edge of the plate is clamped since this quite closely approximates the condition found in several applications of interest. We point out, however, that the techniques which follow are easily adapted to other essential boundary conditions if warranted by the physical model.

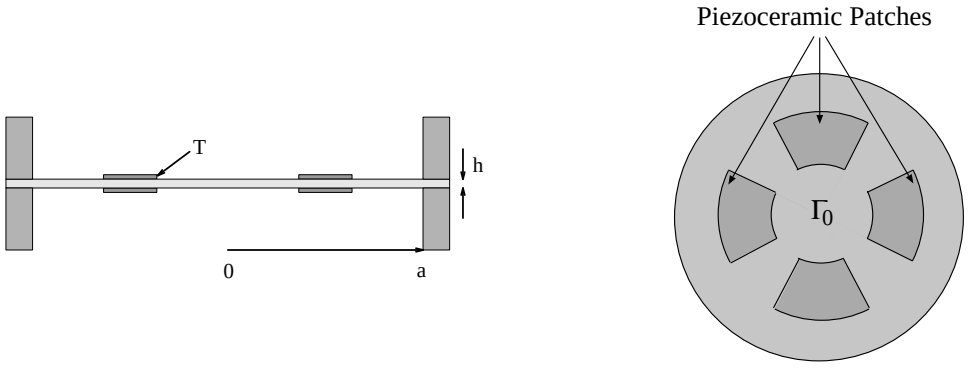

Figure 3. A thin circular plate with piezoeceramic patches bonded in pairs to its surface.

For a thin circular plate of radius a having clamped edges, the strong form of the equations modeling the transverse motion is

$$\begin{aligned} &\rho_p h w_{tt} + \frac{\partial^2 \mathcal{M}_r}{\partial r^2} + \frac{2}{r}\frac{\partial \mathcal{M}_r}{\partial r} - \frac{1}{r}\frac{\partial \mathcal{M}_\theta}{\partial r} + \frac{2}{r}\frac{\partial^2 \mathcal{M}_{r\theta}}{\partial r \partial \theta} + \frac{2}{r^2}\frac{\partial \mathcal{M}_{r\theta}}{\partial \theta} + \frac{1}{r^2}\frac{\partial^2 \mathcal{M}_\theta}{\partial \theta^2} = f(t,r,\theta) \ , \\ &w(t,a,\theta) = \frac{\partial w}{\partial r}(t,a,\theta) = 0 \\ &w(0,r,\theta) = w_0(r,\theta) \quad , \quad w_t(0,r,\theta) = w_1(r,\theta) \end{aligned} \tag{3.1}$$

where ρ_p and h denote the density and thickness of the plate and w is the transverse displacement. The general moments are given by

$$\begin{aligned} \mathcal{M}_r &= M_r - (M_r)_{pe} \\ \mathcal{M}_\theta &= M_\theta - (M_\theta)_{pe} \\ \mathcal{M}_{r\theta} &= M_{r\theta} \end{aligned}$$

where

$$\begin{aligned} M_r &= D\left(\frac{\partial^2 w}{\partial r^2} + \frac{\nu}{r}\frac{\partial w}{\partial r} + \frac{\nu}{r^2}\frac{\partial^2 w}{\partial \theta^2}\right) + c_D\left(\frac{\partial^3 w}{\partial r^2 \partial t} + \frac{\nu}{r}\frac{\partial^2 w}{\partial r \partial t} + \frac{\nu}{r^2}\frac{\partial^3 w}{\partial \theta^2 \partial t}\right) \\ M_\theta &= D\left(\frac{1}{r}\frac{\partial w}{\partial r} + \frac{1}{r^2}\frac{\partial^2 w}{\partial \theta^2} + \nu\frac{\partial^2 w}{\partial r^2}\right) + c_D\left(\frac{1}{r}\frac{\partial^2 w}{\partial r \partial t} + \frac{1}{r^2}\frac{\partial^3 w}{\partial \theta^2 \partial t} + \nu\frac{\partial^3 w}{\partial r^2 \partial t}\right) \\ M_{r\theta} &= D(1-\nu)\left(\frac{1}{r}\frac{\partial^2 w}{\partial r \partial \theta} - \frac{1}{r^2}\frac{\partial w}{\partial \theta}\right) + c_D(1-\nu)\left(\frac{1}{r}\frac{\partial^3 w}{\partial r \partial \theta \partial t} - \frac{1}{r^2}\frac{\partial^2 w}{\partial \theta \partial t}\right) \end{aligned} \tag{3.2}$$

are the internal plate moments (including discontinuous changes in D, ν and c_D due to the bonding of the patches to the plate – see [8]), and

$$(M_r)_{pe} = (M_\theta)_{pe} = \sum_{i=1}^{s} \mathcal{K}_i u_i(t) \chi_i(r,\theta)$$

are the applied moments generated by s pairs of patches. With E denoting the Young's modulus, the parameters $\nu, D = \frac{Eh^3}{12(1-\nu^2)}$ and c_D represent the Poisson ratio, flexural rigidity, and damping coefficient for the plate/patch structure. Here $\chi_i(r,\theta)$ denotes the characteristic function which has a value of 1 in the region covered by the i^{th} patch and is 0 elsewhere. Moreover, $u_i(t)$ is the voltage into the i^{th} patch and $\mathcal{K}_i$ is a parameter which depends on the geometry, piezoceramic material properties and piezoelectric strain constants (see [8] for details). We point out that the piezoceramic material parameters $\mathcal{K}_i, i = 1, \cdots, s$ as well as the plate parameters ρ_p, D, c_D and ν should be considered as unknown and in applications must be estimated using data fitting techniques analogous to those discussed in [7]. The piecewise nature of the material parameters and input moments is one motivation for approximating the problem in a weak or variational form.

To motivate the development of a Fourier-Galerkin scheme for this problem, we proceed in a manner analogous to that used in the last section and consider first a simplified version of the problem where separation of variables can be employed. To this end, we analyze first the equation

$$\rho_p h \frac{\partial^2 w}{\partial t^2} + D\nabla^4 w = 0 \ . \tag{3.3}$$

which models the transverse motion of an undamped thin circular plate devoid of patches and having constant stiffness and density. Because the manner of solution is similar to that discussed in the last section, we highlight only those details which are necessary for motivating the form of the approximate solution for this problem.

As before, we separate the temporal and spatial variables, in this case taking $w(t,r,\theta) = T(t)W(r,\theta)$, to obtain

$$\begin{aligned} \nabla^4 W &= \gamma^4 W \\ W(a,\theta) &= \frac{\partial W}{\partial r}(a,\theta) = 0 \end{aligned} \tag{3.4}$$

and $T'' + \omega^2 T = 0\,, t > 0$. The separation constant is $\gamma^4 = \frac{\rho_p h \omega^2}{D}$ where ω again denotes the circular frequency. A second separation of variables then yields solutions of the form

$$W(r) = A_m J_m(\gamma r) + B_m I_m(\gamma r) + C_m Y_m(\gamma r) + D_m K_m(\gamma r) \tag{3.5}$$

where J_m and Y_m are Bessel functions of the first and second kind and $I_m(z) = i^{-m} J_m(iz)$ and $K_m = lim_{p\to m}\frac{\pi}{2}[I_{-p}(z) - I_p(z)]/\sin(p\pi)$ are modified Bessel functions of the first and second kinds, respectively. We note that for fixed m and $z \to 0$, these functions have the limiting forms

$$\begin{aligned} J_m(z) &\sim \frac{z^m}{2^m m!} & I_m(z) &\sim \frac{z^m}{2^m m!} \\ Y_m(z) &\sim -\frac{2^m (m-1)!}{\pi z^m} & K_m(z) &\sim \frac{2^m (m-1)!}{2 z^m} \end{aligned} \tag{3.6}$$

(see [1]) which immediately shows that the Bessel function and modified Bessel function of the second kind grow unboundedly at the origin. Hence C_m and D_m are taken to be zero in order to avoid infinite deflections and stresses at $r = 0$. Furthermore, the condition $W(a,\theta) = 0$ yields the condition

$$A_m = -B_m \frac{I_m(\lambda)}{J_m(\lambda)} \tag{3.7}$$

where $\lambda \equiv \gamma a$. Finally, the boundary condition $\frac{\partial W}{\partial r}(a,\theta) = 0$ requires that λ solve

$$I_m(\lambda)\frac{dJ_m(\lambda)}{dr} - J_m(\lambda)\frac{dI_m(\lambda)}{dr} = 0 \tag{3.8}$$

in order that (3.5) yields a nontrivial solution to (3.4). By solving (3.8), one obtains the eigenvalues λ_{mn} and by combining (3.5) and (3.7) with the Fourier coefficients, the eigenfunctions or modes are found to be

$$\Psi_m(r,\theta) = \left[J_m\left(\frac{\lambda_{mn} r}{a}\right) - \frac{J_m(\lambda_{mn})}{I_m(\lambda_{mn})} I_m\left(\frac{\lambda_{mn} r}{a}\right)\right] e^{im\theta}\ . \tag{3.9}$$

With suitable smoothness assumptions on the the initial conditions, it then can be shown that the solution to (3.3) has the form

$$w(t,r,\theta) = \sum_{m=-\infty}^{\infty}\sum_{n=1}^{\infty} w_{mn}(t)\left[J_m\left(\frac{\lambda_{mn} r}{a}\right) - \frac{J_m(\lambda_{mn})}{I_m(\lambda_{mn})} I_m\left(\frac{\lambda_{mn} r}{a}\right)\right] e^{im\theta} \tag{3.10}$$

where the coefficients $w_{mn}(t)$ depend on the initial conditions. Again, we note that the motivation given here is formal and we refer the reader to any standard PDE tex for details concerning this derivation.

Having motivated the general form of the analytic solution for a specific case of the plate equation, we can now present a Fourier-Galerkin method for approximating plate dynamics in the more general cases. As noted at the beginning of the section, the weak form of the system equation (3.1) will be used to accommodate potentially discontinuous material parameters. Moreover, the use of the weak form accommodates unbounded input operators (as is the case when piezoceramic patches are used as control elements) as well as reduces the smoothness requirements on the basis functions.

The state for the problem is taken to be w and the Hilbert space $H = L^2(\Gamma_0)$ with the energy inner product

$$\langle w, \eta \rangle_H = \int_{\Gamma_0} \rho_p h w \overline{\eta} d\gamma$$

is used as the state space. We also define the Hilbert space of test functions $V = H_0^2(\Gamma_0) \equiv \{\psi \in H^2(\Gamma_0) : \psi(a,\theta) = \psi'(a,\theta) = 0\}$ with the inner product

$$\langle w, \eta \rangle_V = \left\langle M_r, \frac{\partial^2 \eta}{\partial r^2} \right\rangle + \left\langle \frac{1}{r} M_\theta, \frac{\partial \eta}{\partial r} \right\rangle + \left\langle \frac{1}{r^2} M_\theta, \frac{\partial^2 \eta}{\partial \theta^2} \right\rangle + 2 \left\langle \frac{1}{r} M_{r\theta}, \frac{\partial^2 \eta}{\partial r \partial \theta} \right\rangle - 2 \left\langle \frac{1}{r^2} M_{r\theta}, \frac{\partial \eta}{\partial \theta} \right\rangle$$

where $c_D = 0$ in the moments appearing in this definition and $\langle F, G \rangle = \int_{\Gamma_0} F \overline{G} d\gamma$ with $d\gamma = r dr d\theta$. As detailed in [6], a weak or variational form of the equation describing the motion of a damped thin circular plate having s piezoceramic patch pairs is

$$\begin{aligned} &\int_{\Gamma_0} \rho_p h w_{tt} \overline{\eta} d\gamma + \int_{\Gamma_0} M_r \overline{\frac{\partial^2 \eta}{\partial r^2}} d\gamma + \int_{\Gamma_0} \frac{1}{r} M_\theta \overline{\frac{\partial \eta}{\partial r}} d\gamma + \int_{\Gamma_0} \frac{1}{r^2} M_{r\theta} \left[\overline{\frac{\partial^2 \eta}{\partial \theta^2}} + 2r \overline{\frac{\partial^2 \eta}{\partial r \partial \theta}} - 2 \overline{\frac{\partial \eta}{\partial \theta}} \right] d\gamma \\ &\quad = \int_{\Gamma_0} \sum_{i=1}^{s} \mathcal{K}_i u_i(t) \chi_i(r,\theta) \overline{\nabla^2 \eta} d\gamma + \int_{\Gamma_0} f \overline{\eta} d\gamma \end{aligned} \tag{3.11}$$

for all $\eta \in V$. Again, the internal moments are given in (3.2).

To obtain an appropriate form for the approximate solution, we begin with the Fourier expansion in θ

$$w^{\mathcal{N}}(t,r,\theta) = \sum_{m=-M}^{M} \tilde{w}_m(t,r) e^{im\theta} \ .$$

As was the case when describing the wave approximation, we will use the complex Fourier expansion while describing the method since it simplifies the notation. Due to the potential presence of patches or other actuators on the plate, however, the method is more easily implemented using the real (trigonometric) expansion (with patches present, the complex expansion leads to a complex system matrix which proves troublesome when solving the Riccati equation in the control problem). We have omitted details concerning the real expansions used in the implementation since it is straightforward to interchange between the two expansions.

To determine an appropriate expression for $\tilde{w}_m(t,r)$, we first note that it must satisfy the conditions

$$\tilde{w}_m(t,r) = 0 \ , \ m \neq 0 \quad ; \ \frac{\partial \tilde{w}_0}{\partial r} = 0$$

at $r = 0$ in order to guarantee uniqueness and differentiability (see the discussion about the analogous requirement for the wave solution). In light of these requirements, an appropriate expression for $\tilde{w}_m(t,r)$ is

$$\tilde{w}_m(t,r) = \sum_{n=1}^{N^m} w_{mn}(t) r^{|\hat{m}|} B_n^m(r)$$

where $B_n^m(r)$ is the n^{th} modified cubic spline satisfying $B_n^m(a) = \frac{dB_n^m(a)}{dr} = 0$ with the condition $\frac{dB_n^m(0)}{dr} = 0$ being enforced when $m = 0$ (this latter condition guarantees differentiability at the origin and implies that $N^m = N + 1$ when $m \neq 0$ and $N^m = N$ when $m = 0$, where N denotes the number of modified cubic splines). The total number of plate basis functions is $\mathcal{N} = (2M + 1)(N + 1) - 1$. The inclusion of the weighting term $r^{|\hat{m}|}$ with

$$\hat{m} = \begin{cases} 0 & , \quad m = 0 \\ 1 & , \quad m \neq 0 \end{cases}$$

is motivated by the asymptotic behavior of the Bessel functions (see (3.6)) as $r \to 0$. It also serves to ensure the uniqueness of the solution at the origin. The Fourier coefficient in the weight is truncated to control the conditioning of the mass and stiffness matrices (see examples in [6]).

To simplify notation, the approximate solution is written as

$$w^{\mathcal{N}}(t, r, \theta) = \sum_{m=-M}^{M} \sum_{n=1}^{N^m} w_{mn}(t) r^{|\hat{m}|} B_n^m(r) e^{im\theta} = \sum_{k=1}^{\mathcal{N}} w_k(t) B_k^{\mathcal{N}}(r, \theta) \tag{3.12}$$

where $B_k^{\mathcal{N}}(r, \theta) = r^{|\hat{m}|} B_n^m(r) e^{im\theta}$. A comparison with (3.10) indicates that, as was the case with the wave approximation, the Bessel components of the analytic solution are essentially replaced by approximating elements suitable for the problem under consideration. In the wave problem, the approximate solution was expressed in terms of weighted Legendre polynomials whereas here the radial basis is comprised of weighted cubic splines. In both cases, the weights were used to incorporate the analytic solution behavior at the origin into the approximate solution, thus guaranteeing that it had the correct continuity and differentiability characteristics at that point.

To obtain a corresponding matrix system, the $\mathcal{N}$ dimensional approximating subspace is taken to be $H^{\mathcal{N}} = span\{B_k^{\mathcal{N}}\}$ and the product space for the first-order system is $\mathcal{H}^{\mathcal{N}} \times \mathcal{H}^{\mathcal{N}}$. The restriction of the infinite-dimensional system (3.11) to the space $\mathcal{H}^{\mathcal{N}} \times \mathcal{H}^{\mathcal{N}}$ then yields the matrix equation

$$\begin{bmatrix} K_D^{\mathcal{N}} & 0 \\ 0 & M^{\mathcal{N}} \end{bmatrix} \begin{bmatrix} \dot{\mathcal{W}}^{\mathcal{N}}(t) \\ \ddot{\mathcal{W}}^{\mathcal{N}}(t) \end{bmatrix} = \begin{bmatrix} 0 & K_D^{\mathcal{N}} \\ -K_D^{\mathcal{N}} & -K_{c_D}^{\mathcal{N}} \end{bmatrix} \begin{bmatrix} \mathcal{W}^{\mathcal{N}}(t) \\ \dot{\mathcal{W}}^{\mathcal{N}}(t) \end{bmatrix} + \begin{bmatrix} 0 \\ \tilde{B}_2^{\mathcal{N}} \end{bmatrix} u(t) + \begin{bmatrix} 0 \\ \tilde{F}_2^{\mathcal{N}}(t) \end{bmatrix}$$

$$\begin{bmatrix} K_D^{\mathcal{N}} & 0 \\ 0 & M^{\mathcal{N}} \end{bmatrix} \begin{bmatrix} \mathcal{W}^{\mathcal{N}}(0) \\ \dot{\mathcal{W}}^{\mathcal{N}}(0) \end{bmatrix} = \begin{bmatrix} g_1^{\mathcal{N}} \\ g_2^{\mathcal{N}} \end{bmatrix}$$

where $\mathcal{W}^{\mathcal{N}}(t) = [w_1(t), w_2(t), \cdots, w_{\mathcal{N}}(t)]^T$ denotes the $\mathcal{N} \times 1$ vector containing the approximate state coefficients. The component matrices and vectors are given by

$$\begin{aligned} K_D^{\mathcal{N}} &= K_{D1} + K_{D2} + K_{D3} + K_{D4} + K_{D5} \\ K_{c_D}^{\mathcal{N}} &= K_{c_D 1} + K_{c_D 2} + K_{c_D 3} + K_{c_D 4} + K_{c_D 5} \\ \left[M^{\mathcal{N}}\right]_{\ell,k} &= \int_{\Gamma_0} \rho_p h B_k^{\mathcal{N}} \overline{B_\ell^{\mathcal{N}}} d\gamma \ , \\ \left[\tilde{F}_2^{\mathcal{N}}(t)\right]_\ell &= \int_{\Gamma_0} f \overline{B_\ell^{\mathcal{N}}} d\gamma \quad , \quad \left[\tilde{B}_2^{\mathcal{N}}\right]_{p,j} = \int_{j^{th}patch} \mathcal{K}_j \overline{\nabla^2 B_p^{\mathcal{N}}} d\gamma \\ \left[g_1^{\mathcal{N}}\right]_\ell &= \left\langle w_0, B_\ell^{\mathcal{N}} \right\rangle_V \quad , \quad \left[g_2^{\mathcal{N}}\right]_\ell = \left\langle w_1, B_\ell^{\mathcal{N}} \right\rangle_H \end{aligned} \tag{3.13}$$

where

$$[K_{D1}]_{\ell,k} = \int_{\Gamma_0} D\left[\frac{\partial^2 B_k^{\mathcal{N}}}{\partial r^2} + \frac{\nu}{r}\frac{\partial B_k^{\mathcal{N}}}{\partial r} + \frac{\nu}{r^2}\frac{\partial^2 B_k^{\mathcal{N}}}{\partial \theta^2}\right]\frac{\partial^2 \overline{B_\ell^{\mathcal{N}}}}{\partial r^2}\,d\gamma \ ,$$

$$[K_{D2}]_{\ell,k} = \int_{\Gamma_0} D\left[\frac{1}{r^2}\frac{\partial B_k^{\mathcal{N}}}{\partial r} + \frac{1}{r^3}\frac{\partial^2 B_k^{\mathcal{N}}}{\partial \theta^2} + \frac{\nu}{r}\frac{\partial^2 B_k^{\mathcal{N}}}{\partial r^2}\right]\frac{\partial \overline{B_\ell^{\mathcal{N}}}}{\partial r}\,d\gamma \ ,$$

$$[K_{D3}]_{\ell,k} = \int_{\Gamma_0} D\left[\frac{1}{r^3}\frac{\partial B_k^{\mathcal{N}}}{\partial r} + \frac{1}{r^4}\frac{\partial^2 B_k^{\mathcal{N}}}{\partial \theta^2} + \frac{\nu}{r^2}\frac{\partial^2 B_k^{\mathcal{N}}}{\partial r^2}\right]\frac{\partial^2 \overline{B_\ell^{\mathcal{N}}}}{\partial \theta^2}\,d\gamma \ ,$$

$$[K_{D4}]_{\ell,k} = 2\int_{\Gamma_0} D(1-\nu)\left[\frac{1}{r^2}\frac{\partial^2 B_k^{\mathcal{N}}}{\partial r\partial\theta} - \frac{1}{r^3}\frac{\partial B_k^{\mathcal{N}}}{\partial \theta}\right]\frac{\partial^2 \overline{B_\ell^{\mathcal{N}}}}{\partial r\partial\theta}\,d\gamma \ ,$$

$$[K_{D5}]_{\ell,k} = 2\int_{\Gamma_0} D(1-\nu)\left[-\frac{1}{r^3}\frac{\partial^2 B_k^{\mathcal{N}}}{\partial r\partial\theta} + \frac{1}{r^4}\frac{\partial B_k^{\mathcal{N}}}{\partial \theta}\right]\frac{\partial \overline{B_\ell^{\mathcal{N}}}}{\partial \theta}\,d\gamma$$

with the index ranges are $k, \ell = 1, \cdots, \mathcal{N}$. The matrices $K_{c_D 1} - K_{c_D 5}$ are defined similarly with the inclusion of the parameter c_D in the various integrals. Finally, we remind the reader that ρ_p, D, ν and c_D are piecewise constant in these definitions due to the presence of the patches.

For application purpose, it useful to note that the matrix system for the plate can be written as the Cauchy system

$$\begin{aligned} \dot{y}^{\mathcal{N}}(t) &= A^{\mathcal{N}} y^{\mathcal{N}}(t) + B^{\mathcal{N}} u(t) + G^{\mathcal{N}}(t) \\ y^{\mathcal{N}}(0) &= y_0^{\mathcal{N}} \end{aligned} \tag{3.14}$$

where $y^{\mathcal{N}}(t) = [\mathcal{W}^{\mathcal{N}}(t), \dot{\mathcal{W}}^{\mathcal{N}}(t)] = [w_1(t), \cdots, w_N(t), \dot{w}_1(t), \cdots, \dot{w}_N(t)]$ denotes the $2\mathcal{N} \times 1$ vector containing the generalized Fourier coefficients for the approximate displacement and velocity. In this form, finite-dimensional parameter estimation and control problems can be readily discussed.

3.1 Example 3

As an initial test of the Fourier-Galerkin approximation scheme, we considered the undamped steady state problem

$$\frac{\partial^2 M_r}{\partial r^2} + \frac{2}{r}\frac{\partial M_r}{\partial r} - \frac{1}{r}\frac{\partial M_\theta}{\partial r} + \frac{2}{r}\frac{\partial^2 M_{r\theta}}{\partial r\partial\theta} + \frac{2}{r^2}\frac{\partial M_{r\theta}}{\partial \theta} + \frac{1}{r^2}\frac{\partial^2 M_\theta}{\partial \theta^2} = f(r,\theta)$$

with the moments given by (3.2). In these expressions, the Poisson ratio, flexural rigidity and damping coefficient were taken to be $\nu = \frac{1}{2}$, $D = \frac{4}{3}$ and $c_D = 0$, respectively. The plate radius was taken to be $a = .6$ and the true solution $w(r,\theta) = (\cos(2\pi r/a) - 1)\sin(\theta)$ was used to generate the forcing function

$$\begin{aligned} f(r,\theta) &= \frac{1}{r^4}\Big[3 + \left(-6\pi r/a + 16\pi^3 r^3/a^3\right)\sin(2\pi r/a) \\ &+ \left(-3 + 12\pi^2 r^2/a^2 + 16\pi^4 r^4/a^4\right)\cos(2\pi r/a)\Big]\sin(\theta) \ . \end{aligned}$$

The absolute and relative errors for this example are summarized in Table 5. By choosing a true solution with a known Fourier coefficient, the Fourier limit could be fixed at $M = 1$ and the convergence rate could be observed as the Galerkin limit N was increased. For sufficiently smooth forcing functions, we would expect the method to exhibit $\mathcal{O}(h^4)$ convergence as a result of the cubic spline basis [18, 19]. To check this, asymptotic errors were calculated by dividing the previous relative errors by 16. Since the number of radial basis functions is doubled each time, this provides a means of checking whether or not the expected convergence rate is being maintained. By comparing the results in the 5^{th} and 6^{th} columns of the table, see that $\mathcal{O}(h^4)$ convergence is being exhibited by the method thus providing an initial test in the efficacy of the method.

M	N	$size(A^{\mathcal{N}})$	$\|w_{true} - w_{app}\|$	$\frac{\|w_{true} - w_{app}\|}{\|w_{true}\|}$	Asym. Error
1	5	15×15	$.4362 - 2$	$.2181 - 2$	
1	10	30×30	$.1454 - 2$	$.7269 - 3$	$.1363 - 3$
1	20	60×60	$.6146 - 4$	$.3073 - 4$	$.4543 - 4$
1	40	120×120	$.6717 - 6$	$.3358 - 6$	$.1921 - 5$

Table 5. Absolute and relative errors for approximate solutions for Example 1.

3.2 Example 4

A second means of testing the accuracy and efficiency of the approximation method is by discretizing the eigenvalue problem (3.4) and comparing the approximate eigenvalues and eigenfunctions with analytic values that have been calculated for a simplified structure. This also provides a means of determining analytic values of the natural frequencies of a uniform plate which can then be compared with values obtained numerically and experimentally for structures involving plates to which patches have been bonded [2] and plates that have been incorporated in structural acoustic systems (as described in Section 4).

For a uniform undamped plate to which no patches are bonded, approximation of the eigenvalue problem (3.4) via the Fourier-Galerkin method described in this section yields the generalized matrix eigenvalue problem

$$K_D^{\mathcal{N}} \vartheta^{\mathcal{N}} = \gamma^4 M^{\mathcal{N}} \vartheta^{\mathcal{N}} \tag{3.15}$$

with the mass and stiffness matrices $M^{\mathcal{N}}$ and $K_D^{\mathcal{N}}$ defined in (3.13). The plate dimensions $a = .2286\,m$ $(9\,in)$, $\rho_p = 2700\,kg/m^3$, $h = .00127\,m$ $(.05\,in)$, and parameter choices $E = 7.1 \times 10^{10}\,N/m^2$ and $\nu = .33$ were used which then yields the flexural rigidity $D = 13.6007\,N \cdot m$. We point out that these choices are consistent with the dimensions and parameters of an experimental plate currently being used in the Acoustics Division, NASA Langley Research Center so that the frequencies determined here could be compared with those obtained obtained experimentally (again, see the application in the following section).

By noting the relationship $f = \frac{1}{2\pi}\omega$ where f is the frequency expressed in hertz and ω is the circular frequency, the natural frequencies of the fixed circular plate can be written as

$$f = \frac{1}{2\pi}\left(\frac{\lambda}{a}\right)^2 \sqrt{\frac{D}{\rho_p h}}\,.$$

For the given dimensions and parameter values, several frequencies deriving from the Bessel solutions λ to the nonlinear equation (3.8), as reported on page 8 of [13], are given in Table 6. Approximate frequencies obtained by solving the generalized matrix eigenvalue problem (3.15) with the basis limits $M = 6$ and $N = 24$ are tabulated in Table 7. We point out that in these tables, the Fourier number m can be interpreted as the number of nodal diameters while n is the number of nodal circles, not including the boundary. In comparing the Bessel and Galerkin results in the two tables, it can be seen that the Fourier-Galerkin provides accurate mass and stiffness matrices which translates to accurate approximations to the natural frequencies for the plate. With the basis limits used here, the largest relative error for the frequencies shown here is 8.1×10^{-4} when $m = 3, n = 6$. Moreover, we see that while the definition of $\hat{m}$ in the weighting term $r^{|\hat{m}|}$ changes at $m = 1$, the method loses no accuracy at that point.

To qualitatively test the ability of the Fourier-Galerkin method to accurately approximate the decay of the solution in neighborhoods of the origin for increasing m, we compared the analytic eigenfunctions given by (3.9) with those obtained via the Fourier-Galerkin method with $M = 5$ and $N = 16$. Representative results using the two techniques are plotted in Figures 4 and 5 with additional examples demonstrating the 3-D behavior, corresponding 2-D slices and error results given in [6]. Qualitatively, the shape of the eigenfunctions in the two sets can be seen to be graphically identical and, by comparing the results for the $(m = 5, n = 0)$ mode, it can be seen that the approximation scheme is accurately capturing the behavior of the solution near the origin. In combination with the eigenvalues results listed in the tables, this demonstrates that the approximation method accurately captures the physics of the problem throughout the circular domain with no loss of accuracy resulting at the origin, in spite of the coordinate singularity. Moreover, as demonstrated by the results in the last example, the expected convergence rates are also maintained through the use of the weight $r^{|\hat{m}|}$.

n	$m=0$	$m=1$	$m=2$	$m=3$	$m=4$	$m=5$	$m=6$
0	61.96	128.95	211.56	309.58	422.56	550.38	692.75
1	241.23	368.90	513.02	673.33	849.82	1042.07	1249.92
2	540.46	728.34	932.93	1154.26	1392.14	1646.34	1916.70
3	959.46	1207.39	1472.15	1753.95	2052.63	2367.90	
4	1498.20	1806.12	2131.29	2473.02			
5	2156.69	2524.45	2909.31	3311.57			
6	2934.91	3362.52	3807.60	4269.79			

Table 6. Natural frequencies deriving from the Bessel expansions (in hertz).

n	$m=0$	$m=1$	$m=2$	$m=3$	$m=4$	$m=5$	$m=6$
0	61.96	128.95	211.55	309.52	422.56	550.38	692.75
1	241.23	368.96	513.04	673.40	849.83	1042.08	1249.93
2	540.46	728.35	932.98	1154.31	1392.18	1646.40	1916.79
3	959.50	1207.41	1472.31	1754.16	2052.83	2368.17	
4	1498.37	1806.28	2131.37	2473.57			
5	2157.22	2525.17	2910.49	3313.05			
6	2936.35	3364.46	3810.17	4273.26			

Table 7. Natural frequencies obtained via the Fourier-Galerkin scheme with $M = 6, N = 24$.

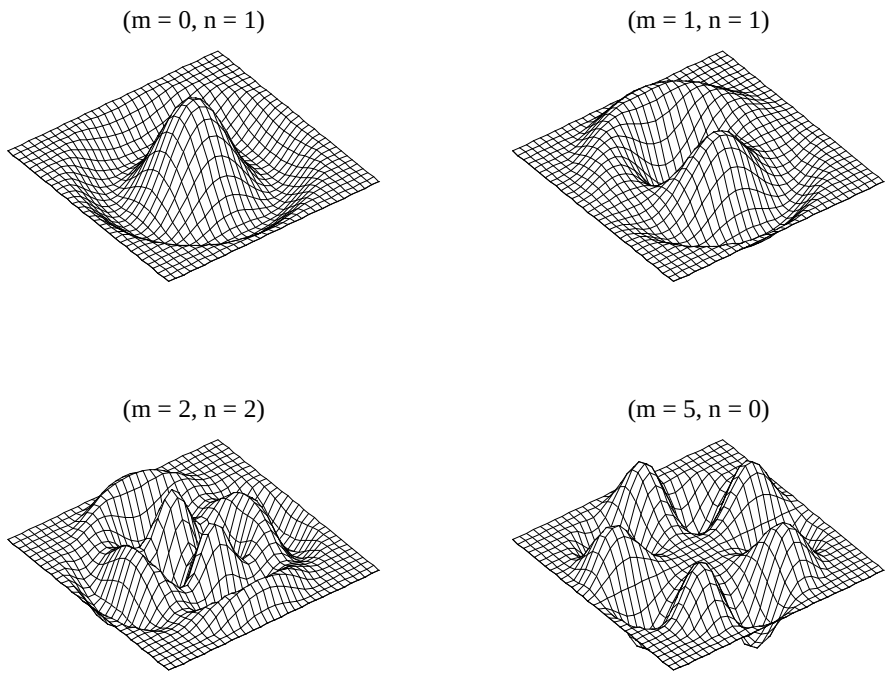

Figure 4. The $(0,1),(1,1),(2,2)$ and $(5,0)$ modes obtained with Bessel expansions.

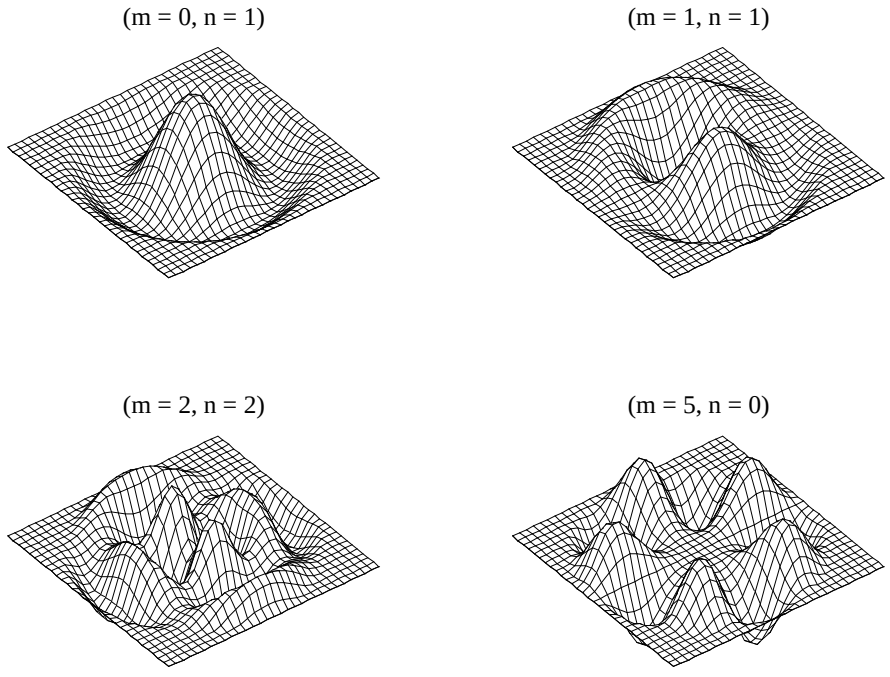

Figure 5. The $(0,1),(1,1),(2,2)$ and $(5,0)$ modes obtained via the Fourier-Galerkin scheme with $M = 5$ and $N = 16$.

4 Application – Structural Acoustic Noise Control

In the previous two sections, Fourier-Galerkin methods for isolated acoustic and structural systems have been developed and illustrated through a set of examples. In this section, a structural acoustic application will be used to demonstrate the manner though which these techniques can be combined to yield an effective approximation scheme for simulating the dynamics of more complex systems. When modeling the experimental setup which motivates this application, care was taken to include the full coupling between the structural dynamics and the enclosed acoustic field, internal damping in the structure, and the effects of actuators such as piezoceramic patches which are bonded to the structure. The full inclusion of these components leads to a model which accurately captures the physics of the system but is difficult to approximate using standard modal techniques since modes for the coupled system (including coupling, damping and actuator effects) must themselves be approximated since they are not known analytically. Using a Fourier-Galerkin technique, however, the approximate system can be directly constructed with several of the components actually consisting of matrices from the isolated acoustic and structural systems. In addition to illustrating the method for the specific setup described here, this demonstrates the flexibility of the method for approximating the dynamics for general structural acoustic systems having circular or cylindrical geometries.

4.1 The Structural Acoustic System

The structural acoustic system described here models an experimental setup currently being used for validation experiments in the Acoustics Division, NASA Langley Research Center, and the geometry and physical specifications were chosen so as to be consistent with that apparatus. Specifically, the experimental apparatus is modeled by a cylindrical domain Ω having length ℓ and radius a as pictured in Figure 6. At one end of the cylinder is a clamped flexible plate of thickness h which is assumed to have Kelvin-Voigt damping. Bonded to the plate are sectorial piezoceramic patches which are placed in pairs and excited out-of-phase so that a bending moment is produced when voltage is appled. The patches and glue layer are assumed to have thicknesses T and $T_{b\ell}$, respectively.

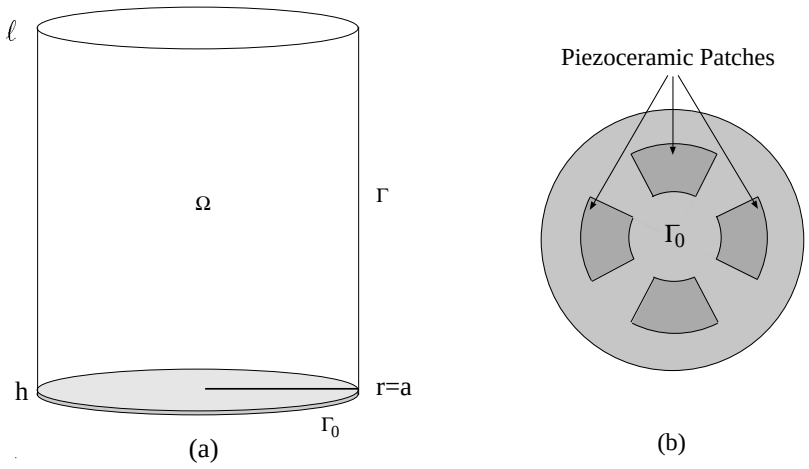

Figure 6. (a) The cylindrical acoustic cavity; (b) The circular plate with patches.

As discussed in [3, 4], an appropriate linearized variational (energy) form of the coupled system equations modeling this setup is

$$\int_\Omega \frac{\rho_f}{c^2}\phi_{tt}\overline{\xi}d\omega + \int_\Omega \rho_f \nabla\phi\cdot\overline{\nabla\xi}d\omega + \int_\Omega g\overline{\xi}d\omega \tag{4.1a}$$

$$+\int_{\Gamma_0}\rho_p h w_{tt}\overline{\eta}d\gamma + \int_{\Gamma_0} M_r\overline{\frac{\partial^2\eta}{\partial r^2}}d\gamma + \int_{\Gamma_0}\frac{1}{r}M_\theta\overline{\frac{\partial\eta}{\partial r}}d\gamma + \int_{\Gamma_0}\frac{1}{r^2}M_{r\theta}\overline{\frac{\partial^2\eta}{\partial\theta^2}}d\gamma \tag{4.1b}$$

$$+2\int_{\Gamma_0}\frac{1}{r}M_{r\theta}\overline{\frac{\partial^2\eta}{\partial r\partial\theta}}d\gamma - 2\int_{\Gamma_0}\frac{1}{r^2}M_{r\theta}\overline{\frac{\partial\eta}{\partial\theta}}d\gamma \tag{4.1b}$$

$$+\int_{\Gamma_0}\rho_f\left(\phi_t\overline{\eta} - w_t\overline{\xi}\right)d\gamma \tag{4.1c}$$

$$=\int_{\Gamma_0}\sum_{i=1}^{s}\mathcal{K}_i^B u_i(t)\chi_i(r,\theta)\overline{\nabla^2\eta}d\gamma + \int_{\Gamma_0} f\overline{\eta}d\gamma \tag{4.1d}$$

for all appropriate test functions ξ and η (this will be clarified below). The differentials here are $d\omega = r\,dr\,d\theta\,dz$ and $d\gamma = r\,dr\,d\theta$ with the overbars again denoting complex conjugation. We now consider the components of the equations and compare with those found previously. Throughout this section, the subscripts p and c will be used to denote plate and wave (cavity) components, respectively.

Acoustic: With $\phi\in\bar{L}^2(\Omega)$ again denoting the acoustic velocity potential, the wave dynamics are contained in (4.1a) where the test functions ξ are elements in $\bar{H}^1(\Omega)$ (see Section 2 for details concerning the Hilbert spaces for this problem). When approximating the dynamics of the system, the 2-D basis described in Section 2 is tensored with an axial Legendre basis to yield the approximate solution

$$\phi^{\mathcal{M}}(t,r,\theta,z) = \sum_{p=0}^{P_c}\sum_{m=-M_c}^{M_c}\sum_{\substack{n=0\\ p+|m|+n\neq 0}}^{N_c^{p,m}} \phi_{pmn}(t)e^{im\theta}r^{|\hat{m}|}P_n^{p,m}(r)P_p(z)$$

where again,

$$\hat{m} = \begin{cases} m & , \quad |m| = 0,\cdots,5 \\ 5 & , \quad |m| = 6,\cdots,M_c \end{cases}$$

and

$$P_n^{p,m}(r) = \begin{cases} P_1(r) - 1/3 & , \quad p = m = 0, n = 1 \\ P_n(r) & , \quad \text{otherwise} \end{cases} \quad , \quad N_c^{p,m} = \begin{cases} N_c + 1 & , \quad p + |m| \neq 0 \\ N_c & , \quad p = m = 0 \end{cases}$$

Here $P_n(r)$ and $P_p(z)$ are the n^{th} and p^{th} Legendre polynomials which have been mapped to the intervals $(0,a)$ and $(0,\ell)$, respectively. We remind the reader that the term $P_1(r)-1/3$ when $p=m=0, n=1$ results from enforcing the condition $\int_\Omega \phi^{\mathcal{M}}(t,r,\theta,z)d\omega = 0$ so as to guarantee that the functions are suitable as a basis for the quotient space while $r^{|\hat{m}|}$ incorporates the analytic decay at the origin with $\hat{m}$ truncated to control conditioning.

Structural: Equation (4.1b) contains the internal plate dynamics while the external contributions due to the perturbing noise source f and the excitation of the patches are contained in (4.1d) (compare with (3.11) in the last section). As was the case when the isolated plate was considered, $w \in L^2(\Gamma_0)$ denotes the transverse displacement and the test functions η are taken in $H_0^2(\Gamma_0)$. When discretizing the system, the plate displacement is approximated by $w^{\mathcal{N}}(t,r,\theta)$ as defined in (3.12) with M_p and N_p used here to denote the Fourier and spline limits, respectively.

Coupling: The coupling between the plate dynamics and interior acoustic field is incorporated by including the backpressure $\rho_f \phi_t(t,r,0)$ from the interior field as a force on the plate and assuming the continuity of velocity condition

$$\frac{\partial \phi}{\partial z}(t,r,\theta,0) = -w_t(t,r,\theta)$$

at the surface of the plate (this latter condition is often designated the momentum condition in the literature). In the weak form of the system equations, these conditions are manifested as the first and second terms, respectively, in (4.1c).

With the components thus described, we are now in a position to form the matrix system which results when the system dynamics are approximated. The $\mathcal{N} = (2M_p+1)(N_p+1)-1$ and $\mathcal{M} = (2M_c+1)(N_c+1)(P_c+1)-1$ dimensional approximating plate and cavity subspaces are taken to be $H_p^{\mathcal{N}} = \text{span}\{B_i^{\mathcal{N}}\}_{i=1}^{\mathcal{N}}$ and $H_c^{\mathcal{M}} = \text{span}\{B_i^{\mathcal{M}}\}_{i=1}^{\mathcal{M}}$, respectively, where $B_i^{\mathcal{N}}$ and $B_i^{\mathcal{M}}$ are the i^{th} plate and cavity bases described above. Defining $\mathcal{P} = \mathcal{N} + \mathcal{M}$, the approximating state space is $H^{\mathcal{P}} = H_c^{\mathcal{M}} \times H_p^{\mathcal{N}}$ and the product space for the first order system is $\mathcal{H}^{\mathcal{P}} = H^{\mathcal{P}} \times H^{\mathcal{P}}$.

The restriction of the infinite-dimensional system (4.1) to $\mathcal{H}^{\mathcal{P}} \times \mathcal{H}^{\mathcal{P}}$ then yields the matrix system

$$\begin{aligned} M^{\mathcal{P}} \dot{y}^{\mathcal{P}}(t) &= \tilde{A}^{\mathcal{P}} y^{\mathcal{P}}(t) + \tilde{B}^{\mathcal{P}} u(t) + \tilde{F}^{\mathcal{P}}(t) \\ M^{\mathcal{P}} y^{\mathcal{P}}(0) &= \tilde{y}_0^{\mathcal{P}} \ . \end{aligned} \tag{4.2}$$

Here $y^{\mathcal{P}}(t) = [\vartheta^{\mathcal{P}}(t), \mathcal{W}^{\mathcal{P}}(t), \dot{\vartheta}^{\mathcal{P}}(t), \dot{\mathcal{W}}^{\mathcal{P}}(t)]^T$, with the components $\vartheta^{\mathcal{P}}(t) = [\phi_1^{\mathcal{P}}(t), \cdots, \phi_{\mathcal{M}}^{\mathcal{P}}(t)]^T$ and $\mathcal{W}^{\mathcal{P}}(t) = [w_1^{\mathcal{P}}(t), \cdots, w_{\mathcal{N}}^{\mathcal{P}}(t)]^T$, denotes the approximate state vector coefficients while $u(t) = [u_1(t), \cdots, u_s(t)]^T$ contains the s patch input variables. The system matrices and vectors are

$$M^{\mathcal{P}} = \left[\begin{array}{cc|cc} K_{r\theta z}^{\mathcal{M}} & & & \\ & K_D^{\mathcal{N}} & & \\ \hline & & M_{r\theta z}^{\mathcal{M}} & \\ & & & M^{\mathcal{N}} \end{array}\right] \quad , \quad \tilde{A}^{\mathcal{P}} = \left[\begin{array}{cc|cc} & & K_{r\theta z}^{\mathcal{M}} & \\ & & & K_D^{\mathcal{N}} \\ \hline -K_{r\theta z}^{\mathcal{M}} & & & -A_{c1}^{\mathcal{P}} \\ & -K_D^{\mathcal{N}} & -A_{c2}^{\mathcal{P}} & -K_{c_D}^{\mathcal{N}} \end{array}\right]$$

and

$$\tilde{B}^{\mathcal{P}} = \left[\begin{array}{cccc} 0 & 0 & 0 & \tilde{B}_2^{\mathcal{N}} \end{array}\right]^T \quad , \quad \tilde{F}^{\mathcal{P}}(t) = \left[\begin{array}{cccc} 0 & 0 & \tilde{G}_2^{\mathcal{M}}(t) & \tilde{F}_2^{\mathcal{N}}(t) \end{array}\right]^T \ .$$

We now separate the matrices into those containing acoustic, structural and coupling components to better illustrate the connections with those developed for the isolated acoustic and structural problems in the previous sections.

Structural: The $\mathcal{N} \times \mathcal{N}$ component matrices $M^{\mathcal{N}}, K_D^{\mathcal{N}}$ and $K_{c_D}^{\mathcal{N}}$ are the mass, stiffness and damping matrices which arise when solving the damped plate equation with fixed boundary conditions while the $\mathcal{N} \times 1$ vectors $\tilde{B}_2^{\mathcal{N}}$ and $\tilde{F}_2^{\mathcal{N}}(t)$ are the corresponding control and forcing terms (see (3.13) for the various definitions).

Acoustic: The $\mathcal{M} \times \mathcal{M}$ matrices $M_{r\theta z}^{\mathcal{M}}$ and $K_{r\theta z}^{\mathcal{M}}$ are the mass and stiffness matrices which arise when solving the uncoupled wave equation with Neumann boundary conditions on a cylindrical domain. As a results of the tensor properties of the 3-D basis, they can be succinctly defined as the tensor products

$$M_{r\theta z}^{\mathcal{M}} = M_z^{\mathcal{M}} \otimes M_{r\theta}^{\mathcal{M}} \ ,$$
$$K_{r\theta z}^{\mathcal{M}} = M_z^{\mathcal{M}} \otimes K_{r\theta}^{\mathcal{M}} + K_z^{\mathcal{M}} \otimes M_{r\theta}^{\mathcal{M}}$$

where $M_{r\theta}^{\mathcal{M}}$ and $K_{r\theta}^{\mathcal{M}}$ are given in (2.15) and the $(P_c + 1) \times (P_c + 1)$ matrices M_z and K_z are defined by

$$[M_z]_{ij} = \int_0^\ell P_i(z) P_j(z) dz \quad , \quad [K_z]_{ij} = \int_0^\ell P_i'(z) P_j'(z) dz \ .$$

The construction of $M_{r\theta z}^{\mathcal{M}}$ and $K_{r\theta z}^{\mathcal{M}}$ is completed by updating the row and column affected by the alterations used to guarantee that the functions are a basis for the quotient space. Finally, $\tilde{G}_2^{\mathcal{M}}(t)$ is a forcing term which incorporates any acoustic sources (see (2.15)).

Coupling: The contributions from the coupling terms are contained in the matrices

$$\left[A_{c1}^{\mathcal{P}}\right]_{\ell,i} = -\rho_f \int_{\Gamma_0} B_i^{\mathcal{N}} \overline{B_\ell^{\mathcal{M}}} d\gamma \quad , \quad \left[A_{c2}^{\mathcal{P}}\right]_{p,k} = \rho_f \int_{\Gamma_0} B_k^{\mathcal{M}} \overline{B_p^{\mathcal{N}}} d\gamma$$

where $B_i^{\mathcal{N}}$ and $B_\ell^{\mathcal{M}}$ are plate and acoustic basis functions, respectively, and the index ranges are $k, \ell = 1, \cdots, \mathcal{M}$ and $i, p = 1, \cdots, \mathcal{N}$.

Initial Conditions: The vector $\tilde{y}_0^{\mathcal{P}} = [g_1^{\mathcal{M}}, g_2^{\mathcal{M}}, g_1^{\mathcal{N}}, g_2^{\mathcal{N}}]^T$ (see (2.15) and (3.13)) contains the projections of the initial values into the approximating finite dimensional subspaces.

We point out that several of the component matrices are identical to those defined when considering the isolated acoustic and structural systems while others can be efficiently constructed from those components through basic operations such as tensor products. In fact, only the coupling matrices $A_{c1}^{\mathcal{P}}$ and $A_{c2}^{\mathcal{P}}$ containing quadrature values for the plate and acoustic bases must be constructed solely for this problem. This potential for decomposition into existing structural, acoustic and coupling matrices also exists for more complex structural acoustic systems when a Fourier-Galerkin approximation scheme is used and is a further advantage of the method in coupled problems involving linear or weakly nonlinear components.

4.2 Example 5

As a first test demonstrating the convergence of the method for the fully coupled system, we considered the problem (4.1) with the dimensions $a = .6, h = .00127, \ell = 1.1$ and parameter choices $\rho_f = 1.21, c = 343, \rho_p = 2700, \nu = .33, D = \frac{Eh^3}{12(1-\nu^2)} = 13.6007$ and $c_D = .00011222$ (the

effects of the patches are neglected in this example but will be incorporated in Example 6). The true solutions

$$w(r,\theta) = t^3(\cos(2\pi r/a) - 1)\sin\theta$$
$$\phi(t,r,\theta,z) = -\tfrac{3}{\ell^2}t^2(\cos(2\pi r/a) - 1)z(\ell - z)^2\sin\theta$$

were used to generate forcing functions f and g on the plate and in the cavity, respectively (see the convergence tests in Sections 2 and 3). The resulting matrix system (4.2) was then integrated to time $T = .1$ and the absolute and relative errors in the plate displacement, potential and pressure at that time were calculated. The results for four sets of Galerkin limits are reported in Tables 8, 9 and 10. In these tables, the subscripts p and c in the tables again refer to the plate and wave (cavity) indices, respectively, and the measurements were made on a 30×30 grid on the plate and a $10 \times 10 \times 10$ grid in the cavity. As demonstrated by these results, the method for the fully coupled system is exhibiting a convergence rate similar to that noted when the individual components were tested. Moreover, sufficient accuracy is obtained with tractable matrix sizes so that physical details are captured when the approximation method is used to simulate system dynamics and develop feedback control techniques. Finally, we point out that in spite of the fact that we are approximating nonaxisymmetric solutions, the computations for this example could be performed on a Sparc10-class workstation.

M_p	N_p	M_c	N_c	P_c	$size(\tilde{A}^{\mathcal{P}})$	$\|w_{true} - w_{app}\|$	$\frac{\|w_{true}-w_{app}\|}{\|w_{true}\|}$
1	5	1	2	2	86×86	$.4366 - 5$	$.2207 - 2$
1	5	1	4	4	182×182	$.4294 - 5$	$.2171 - 2$
1	10	1	6	6	356×356	$.2674 - 6$	$.1352 - 3$
1	20	1	8	8	608×608	$.1588 - 7$	$.8030 - 5$

Table 8. Absolute and Relative Errors in Plate Displacement at $T = .1$.

M_p	N_p	M_c	N_c	P_c	$size(\tilde{A}^{\mathcal{P}})$	$\|\phi_{true} - \phi_{app}\|$	$\frac{\|\phi_{true}-\phi_{app}\|}{\|\phi_{true}\|}$
1	5	1	2	2	86×86	$.3132 - 2$	$.3569 - 0$
1	5	1	4	4	182×182	$.1545 - 3$	$.1760 - 1$
1	10	1	6	6	356×356	$.9554 - 5$	$.1089 - 2$
1	20	1	8	8	608×608	$.2251 - 6$	$.2565 - 4$

Table 9. Absolute and Relative Errors in Potential at $T = .1$.

M_p	N_p	M_c	N_c	P_c	$size(\tilde{A}^{\mathcal{P}})$	$\|p_{true} - p_{app}\|$	$\frac{\|p_{true}-p_{app}\|}{\|p_{true}\|}$
1	5	1	2	2	86×86	$.7573 - 1$	$.3566 - 0$
1	5	1	4	4	182×182	$.3739 - 2$	$.1761 - 1$
1	10	1	6	6	356×356	$.2312 - 3$	$.1089 - 2$
1	20	1	8	8	608×608	$.5453 - 5$	$.2568 - 4$

Table 10. Absolute and Relative Errors in Pressure at $T = .1$.

4.3 Example 6

In this final example, the numerical techniques just described are used to simulate the system dynamics of the experimental structure described at the beginning of this section. A common technique for determining the dynamics and natural frequencies of coupled structural acoustic systems is to subject the structure to an impulse (through an impact hammer hit or a voltage spike to the patch) and measure the resulting time and frequency responses. By exciting the system in this manner, a wide spectrum of frequencies can be excited and various system properties determined. Because there is no acoustic source inside the cavity, $g \equiv 0$ in (4.1a).

The hammer impact can be numerically simulated by a triangular force f to a point on the plate while the voltage spike can be approximated by a short duration triangular voltage u; in both cases, the approximate system response is calculated via (4.2).

In order to remain consistent with the experimental setup being modeled, the length and radius of the cavity were taken to be $1.0668\,m$ $(42'')$ and $a = .2286\,m$ $(9'')$, respectively with a plate having thickness $h = .00127\,m$ $(.05'')$ mounted at one end. A pair of circular piezoceramic patches having thickness $T = .0001778\,m$ $(.007'')$ and radius $rad = .01905\,m$ $(.75'')$ were located at the center of the plate (see Figure 7). The physical parameters that were chosen for the structure and acoustic cavity are summarized in Table 11. The flexural rigidity D for the plate was obtained using the "handbook" value $E = 7.1 \times 10^{10}\,N/m^2$ for the Young's modulus of aluminum. The remaining choices are comparable to values found when estimating parameters for the isolated plate with a similar patch configuration [2]. We re-emphasize that in general, these parameters must be determined through parameter estimation techniques in order for the PDE model to fit the actual physical system under consideration. As demonstrated in [2], the Fourier-Galerkin scheme presented here performed well when incorporated in a fit-to-data routine for determining physical plate parameters thus yielding a model which could be used for implementing model-based feedback control techniques.

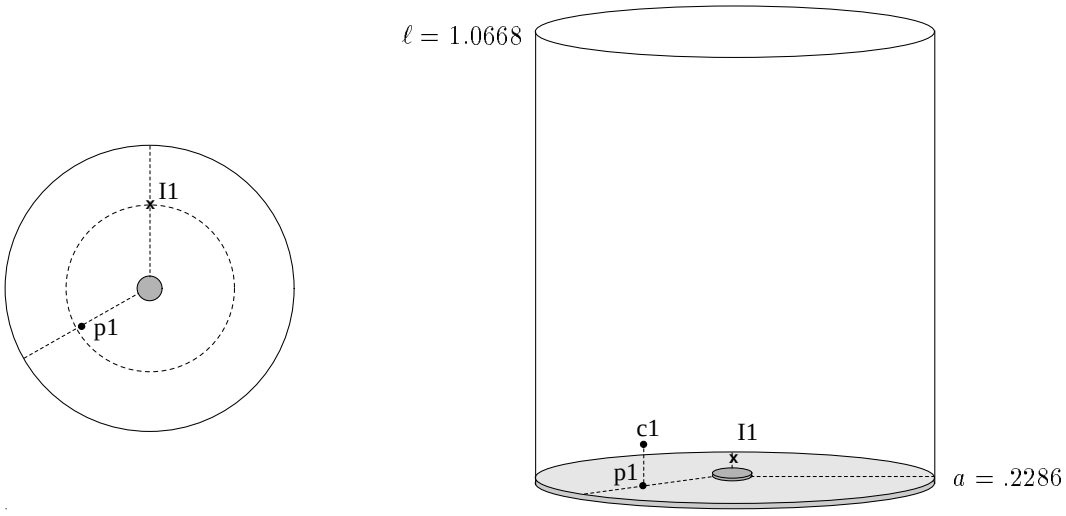

Figure 7. The acoustic cavity with a pair of centered circular patches, the impact point $I1 = (.13, \frac{\pi}{2})$ and the observation points $p1 = (.125, \frac{4\pi}{3})$ and $c1 = (.125, \frac{4\pi}{3}, .05)$.

Structure			Acoustic Cavity	
Parameter	Plate	Plate + Pzt	Parameter	Cavity
$\rho_p \cdot Thickness\ (kg/m^2)$	3.429	3.489	$\rho_f\ (kg/m^3)$	1.21
$D\ (N \cdot m)$	13.601	13.901		
$c_D\ (N \cdot m \cdot sec)$	1.150-4	2.250-4		
ν	.33	.32		
$\mathcal{K}^B\ (N/V)$		.0267		
			c (m/sec)	343

Table 11. Physical Parameters for the structure and acoustic cavity.

Voltage Spike to a Centered Patch Pair – Axisymmetric Response

As a first example demonstrating the response of the system model to a simulated impact, we applied a triangular voltage spike $u(t)$ as input to the patches and integrated the matrix system to obtain a time history of the response. Because the patches are centered on the plate, the response was uniform in θ which implied that the Fourier limits could be taken to be $M_p = M_c = 0$. The remaining limits were taken to be $N_p = 12, N_c = 9$ and $P_c = 9$ (these values resolve the range of frequencies being examined). A time history of the system response throughout the interval $[0, .5]$ was calculated at the plate and cavity points $p1 = (.125, \frac{4\pi}{3})$ and $c1 = (.125, \frac{4\pi}{3}, .05)$ (see Figure 7), and the resulting trajectories and frequencies are plotted in Figure 8. This temporal interval was chosen since it was sufficiently long so as to demonstrate the system dynamics but short enough so that the higher frequency responses were not completely lost. The off-center observation points were chosen to demonstrate the generality of the method and provide a basis for comparison with the nonaxisymmetric results in the next example. Finally, the system frequencies are summarized in Table 12 with the notation p and c being used to designate those frequencies which are observed at the plate point $p1$ and cavity point $c1$, respectively.

To determine the effects of coupling, internal plate damping, and the presence of the patches on the system, it is illustrative to compare the system results listed in Table 12 with those of the isolated components. In Section 3, the natural frequencies for an isolated and undamped plate were obtained. The natural frequencies for the isolated wave equation in a cylindrical cavity can be determined by separating variables in the 3-D wave equation having Neumann boundary conditions. This leads to a 3-D Helmholz equation which, after an analysis similar to that presented in Section 2, yields the natural frequencies

$$f_{mnp} = \frac{1}{2\pi} c \sqrt{\left(\frac{p\pi}{\ell}\right)^2 + \left(\frac{\lambda_{mn}}{a}\right)^2} \tag{4.3}$$

where $p = 1, 2, \cdots$, $m = 0, 1, 2, \cdots$, $n = 0, 1, 2, \cdots$ and $\lambda_{mn} = \gamma_{mn} a$ are zeros of (2.6) (see [3, 6, 9] for details). For the previously mentioned dimensions, the frequencies of axisymmetric modes ($m = 0$) are listed along with those for the isolated and undamped plate in Table 13 (see Tables 2 and 6 for a compilation of the zeros γ_{mn} and natural frequencies for the isolated plate, respectively).

By comparing the values for the individual plate and cavity in Table 13, with the system harmonics in Table 12, it can be seen that although the frequencies agree quite closely, there are slight differences due to the fact that the system (4.1) involves not only coupling between the plate and cavity but also includes damping in the plate. Specifically, the system frequencies associated with strong plate responses tend to be slightly less than those of the uncoupled and undamped plate while those system frequencies associated with strong acoustic responses are slightly higher than the natural acoustic frequencies of an isolated hardwalled cavity having these dimensions. Hence, through the Fourier-Galerkin method, physical characteristics about the system are determined and differences between the coupled system response which includes damping and the isolated, undamped components are illustrated. This latter observation also indicates the difficulties which would be encountered if one were to attempt to simulated the coupled system dynamics using modes for the isolated systems.

Natural System Frequencies					
p,c	59	p,c	164	c	915
p	240	p,c	324	c	929
p,c	537	p,c	483	c	971
		c	645		
		c	807		

Table 12. System frequencies obtained with $M_p = 0, N_p = 12, M_c = 0, N_c = 9$ and $P_c = 9$ basis functions; p – frequencies observed at the plate point $p1 = (.125, 4\pi/3)$, c – frequencies observed at the cavity point $c1 = (.125, 4\pi/3, .05)$. System frequencies can be compared with the ordered frequencies of the isolated and undamped plate and cavity given in Table 13.

Plate (f_{mn})		Wave (f_{mnp})			
(0,0)	62	(0,0,1)	161	(0,1,0)	915
(0,1)	241	(0,0,2)	322	(0,1,1)	929
(0,2)	540	(0,0,3)	482	(0,1,2)	970
(0,3)	959	(0,0,4)	643		
		(0,0,5)	804		
		(0,0,6)	965		

Table 13. Axisymmetric natural frequencies for the isolated and undamped plate and cavity (in hertz).

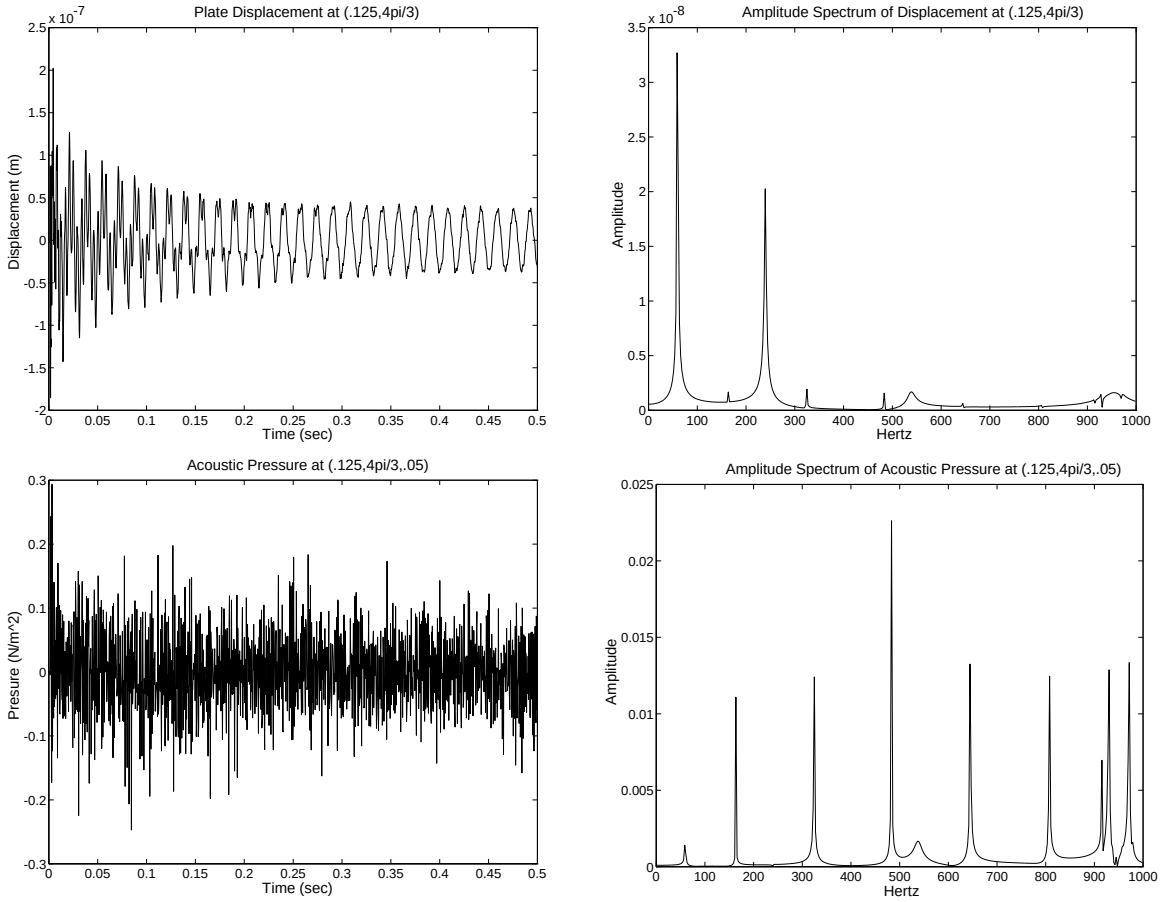

Figure 8. The plate and pressure responses to a voltage spike.

Noncentered Hammer Impact – Non-axisymmetric Response

As indicated previously, a second means of exciting the system is through a hammer impact which can be modeled by a short triangular input force. To demonstrate the approximation of general nonaxisymmetric system dynamics, this force impulse was applied at the point $I1 = (.130, \frac{\pi}{2})$, and a time history of the system response for the time interval $[0, .5]$ was calculated at the plate and cavity points $p1 = (.125, \frac{4\pi}{3})$ and $c1 = (.125, \frac{4\pi}{3}, .05)$, respectively (see Figure 7). The resulting acoustic pressure and plate acceleration are plotted along with the corresponding frequency responses in Figure 9 (the plate acceleration models data that would be experimentally obtained with an accelerometer, [2], and more clearly demonstrates the higher frequencies than does the plate displacement). To resolve the frequencies below 1000 hertz, the basis limits were taken to be $M_p = 4, N_p = 12, M_c = 2, N_c = 9$ and $P_c = 9$ which yielded 1230 coefficients in the system (4.2). As demonstrated by this choice of limits, the number of Fourier coefficients in the plate and wave expansions can be chosen to differ in order to reduce system sizes although care must be taken when doing so since the system response contains contributions from both the plate and wave components.

The system frequencies are summarized in Table 14 where again, the notation p and c are used to designate those frequencies which are observed at the plate and cavity point $p1$ and $c1$, respectively. For comparison, corresponding natural frequencies for an isolated and undamped

plate (see Table 6) and an isolated acoustic cavity (see (4.3)) are compiled in Table 15. By comparing the results in these table, it can be noted that six system modes corresponding to those of the isolated plate are excited with four of these responses being observed at both the plate and cavity points (we emphasize that because these are truly system modes, the remaining frequencies of 240 hertz and 422 hertz can also be measured in the cavity at various points; the response is simply weak at the point $c1$). Similarly, nineteen system modes corresponding to those of the isolated acoustic cavity are excited by the nonsymmetric impact with the strongest response in the asymmetric system mode having a frequency of 460 hertz (this corresponds to the $(1,0,0)$ mode for the isolated cavity). As was noted in the previous example demonstrating the symmetric excitation, the system frequencies associated with strong plate responses tend to be slightly less than those of the uncoupled and undamped plate while those system frequencies associated with strong acoustic responses are slightly higher than the natural acoustic frequencies of an isolated hardwalled cavity having commensurate dimensions. We reiterate that these differences are due to the coupling between the plate and cavity as well as damping in the plate. This again provides motivation for considering a general Fourier-Galerkin method of the type described here when approximating the dynamics of a complex coupled system. The effect of coupling and damping are implicitly included in this approach while they must be explicitly (and occasionally artificially) enforced when employing modal approaches using the eigenfunctions of the isolated components.

Natural Frequencies of the Coupled Structural Acoustic System									
p,c	59	p,c	209	c	164	c	929	c	915
p	240			p,c	324	c	971	c	730
				p,c	483	p,c	440	c	748
				c	645	p,c	470	c	798
p,c	127			c	807	p,c	546	p,c	875
p,c	365	p	422			p,c	653	c	971
				c	915	c	781		

Table 14. System frequencies obtained with $M_p = 4, N_p = 12, M_c = 2, N_c = 9$ and $P_c = 9$ basis functions; p – frequencies observed at the plate point $p1 = (.125, 4\pi/3)$, c – frequencies observed at the cavity point $c1 = (.125, 4\pi/3, .05)$. System frequencies can be compared with the ordered frequencies of the isolated and undamped plate and cavity given in Table 15.

Plate (f_{mn})				Wave (f_{mnp})					
(0,0)	62	(2,0)	212	(0,0,1)	161	(0,1,1)	929	(1,0,5)	916
(0,1)	241	(2,1)	513	(0,0,2)	322	(0,1,2)	970	(2,0,0)	729
(0,2)	540	(2,1)	933	(0,0,3)	482	(1,0,0)	439	(2,0,1)	750
(0,3)	959	(3,0)	310	(0,0,4)	643	(1,0,1)	468	(2,0,2)	797
(1,0)	129	(3,1)	673	(0,0,5)	804	(1,0,2)	545	(2,0,3)	874
(1,1)	369	(4,0)	423	(0,0,6)	965	(1,0,3)	653	(2,0,4)	972
(1,2)	728	(4,1)	850	(0,1,0)	915	(1,0,4)	779		

Table 15. Nonaxisymmetric natural frequencies for the isolated and undamped plate and cavity (in hertz).

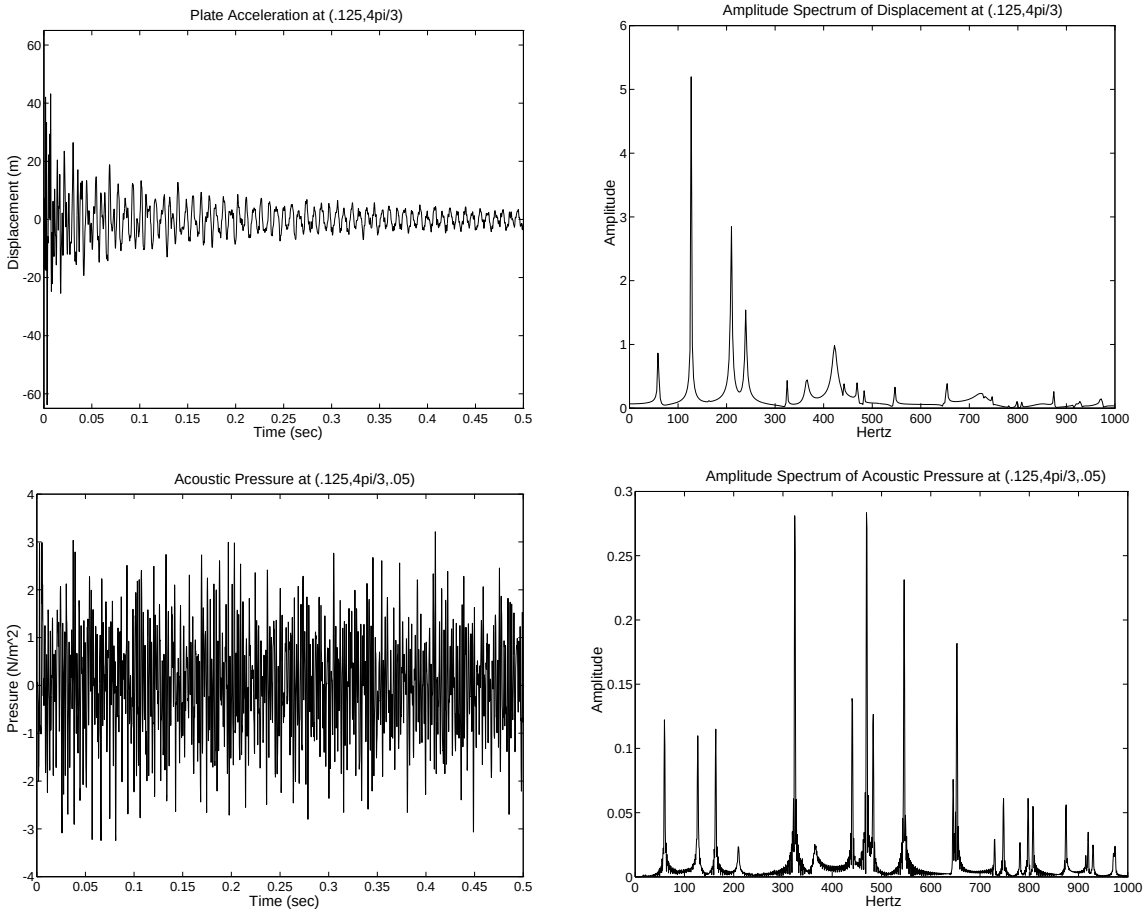

Figure 9. The plate and pressure responses to an impact at $(.13, \pi/2)$.

5 Concluding Remarks and Control Applications

In this paper, a Galerkin method for approximating the dynamics of linear or weakly nonlinear systems in circular geometries is presented. While the method is presented for linear acoustic, structural and structural acoustic problems, the techniques are sufficiently general so as to be applicable in a large variety of applications involving the approximation of linear or weakly nonlinear operators on circular domains.

To take advantage of periodicity, Fourier expansions are first used to approximate the tangential behavior of the solution. The crux of the method then involves the construction of radial basis functions by combining traditional approximating functions (finite elements, piecewise splines, spectral polynomials) with terms of the form $r^{|\hat{m}|}$ where $\hat{m}$ is a truncated Fourier coefficient and the coordinate singularity is assumed to be at the origin. This latter term incorporates the decay properties of the Bessel or analytic solution near the origin and is included so as to guarantee that the approximate solution is unique and differentiable at the coordinate singularity. The truncation of the Fourier coefficient provides a means of controlling the conditioning of the resulting matrix system.

As demonstrated by several numerical examples, the resulting Fourier-Galerkin technique is accurate, efficient and sufficiently flexible so as to be easily extended to complex coupled

systems. By varying the choice of radial basis functions, the method can be tailored to a variety of applications and boundary conditions while the inclusion of the decay component $r^{|\hat{m}|}$ guarantees that accuracy is maintained throughout the entire circular domain for sufficiently smooth system inputs. Hence the Legendre polynomials and modified cubic splines, used in this presentation to approximate acoustic and structural dynamics, can easily be replaced by other spectral functions, splines or finite elements as warranted by the situation.

A final advantage of the method arises when the Fourier-Galerkin techniques are used to compute feedback gains in optimal control problems. As discussed in [5], where the method was incorporated in a control scheme for reducing noise in a cylindrical coupled structural acoustic system, the optimal control problem for reducing a periodically driven state z in the state space $\mathcal{H}$ can be posed under approximation as that of determining a suitable u in a control space U which minimizes

$$J^{\mathcal{P}}(u) = \frac{1}{2}\int_0^\tau \left\{ \langle Q^{\mathcal{P}} z^{\mathcal{P}}(t), z^{\mathcal{P}}(t)\rangle_{\mathbb{R}^{\mathcal{P}}} + \langle R^{\mathcal{P}} u(t), u(t)\rangle_U \right\} dt \tag{5.1}$$

subject to $z^{\mathcal{P}}$ satisfying the matrix system of dimension $\mathcal{P}$ which results when the equations modeling the system dynamics are discretized. Here τ is the period and $Q^{\mathcal{P}}$ and $R^{\mathcal{P}}$ are matrices which can be used to weight various components of the approximate state and control. As noted in [5], a suitable choice for $Q^{\mathcal{P}}$, when an energy inner product is associated with the state space $\mathcal{H}$, is a diagonal multiple of the mass matrix $M^{\mathcal{P}}$ which results when a Galerkin method is used to discretize the weak form of the system equations. Since the mass matrix constructed in this manner is the identity with respect to the energy inner product, the choice $Q^{\mathcal{P}} = \mathcal{D}M^{\mathcal{P}}$, $\mathcal{D}$ a diagonal weighting matrix, in (5.1) minimizes a weighted measure of the state energy. Hence a Fourier-Galerkin method of the type described here can also be advantageous when calculating feedback gains for experimental and numerical implementation of optimal control techniques to problems posed on circular geometries.

ACKNOWLEDGEMENTS:

The author expresses sincere appreciation to H.T. Banks, North Carolina State University, D. Gottlieb, Brown University, R.J. Silcox, Acoustics Division, NASA Langley Research Center and Yun Wang, Center for Research in Scientific Computing, North Carolina State University, for input regarding the modeling, approximation and implementation techniques used in this paper.

References

[1] M. Abramowitz and I.A. Stegan, Editors, *Handbook of Mathematical Functions with Formulas, Graphs, and Mathematical Tables*, Dover Publications, New York, 1972.

[2] H.T. Banks, D.E. Brown, V. Metcalf, R.J. Silcox, R.C. Smith and Y. Wang, "A PDE-Based Methodology for Modeling, Parameter Estimation and Feedback Control in Structural and Structural Acoustic Systems," to appear in the *Proceedings of the 1994 North American Conference on Smart Structures and Materials*, Orlando, FL.

[3] H.T. Banks, R.J. Silcox and R.C. Smith, "Numerical Simulations of a Coupled 3-D Structural Acoustics System," *Proceedings of the Second Conference on Recent Advances in Active Control of Sound and Vibration*, Blacksburg, VA, pp. 85-97, 1993.

[4] H.T. Banks and R.C. Smith, "Modeling and Approximation of a Coupled 3-D Structural Acoustics Problem," *Computation and Control III,* Proceedings of the Third Bozeman Conference, Bozeman, MT, 1992, Progress in Systems and Control Theory, Vol. 15, Birkhäuser Boston, Inc., pp. 29-48, 1993.

[5] H.T. Banks and R.C. Smith, "Noise Control in a 3-D Structural Acoustic System: Numerical Simulations," to appear in the Proc. of the Second International Conference on Intelligent Materials, Williamsburg, VA, 1994.

[6] H.T. Banks and R.C. Smith, "The Modeling and Approximation of a Structural Acoustics Problem in a Hard-Walled Cylindrical Domain," to appear as a Center for Research in Scientific Computation Technical Report.

[7] H.T. Banks and R.C. Smith, "Parameter Estimation in a Structural Acoustic System with Fully Nonlinear Coupling Conditions," submitted to *Inverse Problems.*

[8] H.T. Banks, R.C. Smith and Y. Wang, "Modeling Aspects for Piezoceramic Patch Activation of Shells, Plates and Beams," Center for Research in Scientific Computation Technical Report, CRSC-TR92-12, N. C. State Univ., *Quarterly of Applied Mathematics*, to appear.

[9] R.D. Blevins, *Formulas For Natural Frequency and Mode Shape*, Van Nostrand Reinhold Company, New York, 1979.

[10] S. Bouaoudia and P.S. Marcus, "Fast and Accurate Spectral Treatment of Coordinate Singularities," *Journal of Computational Physics*, 96, 217-223, 1991.

[11] C. Canuto, M.Y. Hussaini, A. Quarteroni and T.A. Zang, *Spectral Methods in Fluid Dynamics*, Springer-Verlag, New York, 1988.

[12] D. Gottlieb and S.A. Orszag, *Numerical Analysis of Spectral Methods: Theory and Applications*, SIAM, Philadelphia, 1977.

[13] A.W. Leissa, *Vibration of Plates,* NASA SP-160, Washington, D.C., 1969.

[14] P.M. Morse and K.U. Ingard, *Theoretical Acoustics,* McGraw-Hill, New York, 1968.

[15] S.A. Orszag, "Fourier Series on Spheres," *Monthly Weather Review*, 102, 56-75, 1974.

[16] S.A. Orszag and A.T. Patera, "Secondary Instability of Wall-Bounded Shear Flows," *Journal of Fluid Mechanics*, 128, 347-385, 1983.

[17] A.T. Patera and S.A. Orszag, "Finite-Amplitude Stability of Axisymmetric Pipe Flow," *Journal of Fluid Mechanics*, 112, 467-474, 1981.

[18] P.M. Prenter, *Spline and Variational Methods,* Wiley-Interscience, New York, 1975.

[19] M.H. Schultz, *Spline Analysis,* Prentice-Hall, Englewood Cliffs NJ, 1973.